Real-time 3D Neural Facial Animation from Binocular Video

CHEN CAO, Facebook Reality Labs, USA
VASU AGRAWAL, Facebook Reality Labs, USA
FERNANDO DE LA TORRE, Facebook Reality Labs, USA
LELE CHEN, Facebook Reality Labs and Univeristy of Rochester, USA
JASON SARAGIH, Facebook Reality Labs, USA
TOMAS SIMON, Facebook Reality Labs, USA
YASER SHEIKH, Facebook Reality Labs, USA

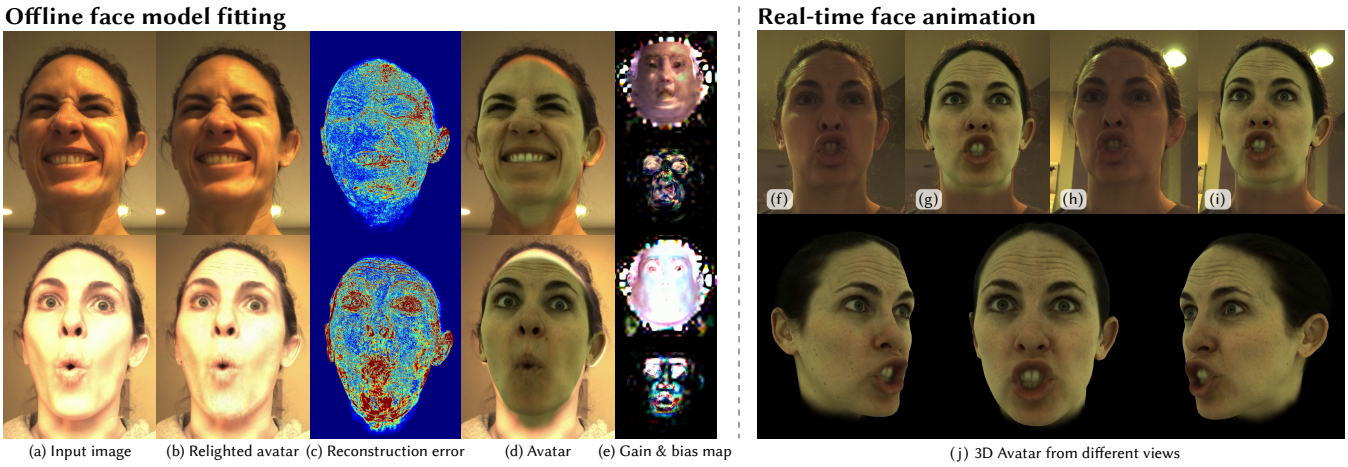

Fig. 1. We present a real-time high-fidelity 3D facial animation method. In the offline face estimation step (a-e), given an input image (a) and a person-specific deep appearance model (PS-DAM), we estimate the model parameters with an analysis-by-synthesis method and track the avatar (d). We propose a new illumination model (i.e., gain and bias map (e)) to relight the avatar (b) and to match the input image (a). We show the L_2 error between (a) and (b) as the reconstruction error in (c). In the online (real-time) facial animation step (f-j), we have a pair of images as input (f,h) and we can accurately track the face and drive the 3D avatar (g,i). The animated 3D avatar across different views is shown in (j).

We present a method for performing real-time facial animation of a 3D avatar from binocular video. Existing facial animation methods fail to automatically capture precise and subtle facial motions for driving a photo-realistic 3D avatar "in-the-wild" (i.e., variability in illumination, camera noise). The novelty of our approach lies in a light-weight process for specializing a personalized face model to new environments that enables extremely accurate real-time face tracking anywhere. Our method uses a pre-trained high-fidelity personalized model of the face that we complement with a novel *illumination model* to account for variations due to lighting and other factors often encountered in-the-wild (e.g., facial hair growth, makeup, skin blemishes). Our approach comprises two steps. First, we solve for our illumination model's parameters by applying analysis-by-synthesis on a short video recording. Using the pairs of model parameters (rigid, non-rigid) and the original images, we learn a regression for real-time inference from the image space to the 3D shape and texture of the avatar. Second, given a new video, we fine-tune the real-time regression model with a few-shot learning strategy to adapt the regression model to the new environment. We demonstrate our system's ability to precisely capture subtle facial motions in unconstrained scenarios, in comparison to competing methods, on a diverse collection of identities, expressions, and real-world environments.

CCS Concepts: • **Computing methodologies** → **Motion capture**; **Mixed / augmented reality**.

Additional Key Words and Phrases: Facial animation, Facial modeling, Differentiable rendering, Augmented reality

ACM Reference Format:
Chen Cao, Vasu Agrawal, Fernando De la Torre, Lele Chen, Jason Saragih, Tomas Simon, and Yaser Sheikh. 2021. Real-time 3D Neural Facial Animation from Binocular Video. *ACM Trans. Graph.* 40, 4, Article 87 (August 2021), 17 pages. https://doi.org/10.1145/3450626.3459806

Authors' addresses: Chen Cao, zju.caochen@gmail.com, Facebook Reality Labs, Pittsburgh, Pennsylvania, USA; Vasu Agrawal, vasuagrawal@fb.com, Facebook Reality Labs, Pittsburgh, Pennsylvania, USA; Fernando De la Torre, ftorre@cs.cmu.edu, Facebook Reality Labs, Pittsburgh, Pennsylvania, USA; Lele Chen, lchen63@cs.rochester.edu, Facebook Reality Labs and Univeristy of Rochester, USA; Jason Saragih, jsaragih@fb.com, Facebook Reality Labs, Pittsburgh, Pennsylvania, USA; Tomas Simon, tomas.simon@oculus.com, Facebook Reality Labs, Pittsburgh, Pennsylvania, USA; Yaser Sheikh, yasers@fb.com, Facebook Reality Labs, Pittsburgh, Pennsylvania, USA.

0730-0301/2021/8-ART87
https://doi.org/10.1145/3450626.3459806

1 INTRODUCTION

Markerless facial motion capture has been a long-standing computer graphics and computer vision problem over the last three decades.

In many applications, such as animating characters in movies or systems to promote a sense of social presence in AR/VR, driving avatars from video with high-degree of photo-realism is required. In these scenarios, a major challenge is to be able to transfer subtle expressions (e.g., perfect eye contact, lip-chewing, tongue movement, blinking) in real-time under a variety of lighting conditions.

There are two main technical challenges: first, we need to correctly decouple rigid (i.e., 3D head pose) and non-rigid motion (i.e., facial expression). Second, we need to render the user's appearance in the avatar. To decouple the rigid/non-rigid motion, a necessary component is a precise facial tracking/alignment mechanism that achieves sub-pixel accuracy. Precise and dense facial feature tracking is challenging in natural scenarios due to sensor noise and variability in lighting. Lighting changes always dominate the marginal information for detail facial information. If we try to decouple the illumination from an image, we usually destroy the information required for subtle facial motions. To render user's appearance in the avatar, in the early days, there were a variety of face tracking methods that use no-model or only shape model for facial animation (e.g., [Decarlo and Metaxas 2000]), but these methods failed catastrophically to recover important facial details such as the interior of the mouth or blinking of the eyes. Alternatively, parametric face models such as Active Appearance Models, Morphable Models, or Deep Appearance Models jointly model the 2D/3D shape and appearance allowing a more precise registration/alignment between the image and the model. In addition, these methods perform tracking by reconstruction with the additional benefit of having a latent code for reconstructing the appearance, providing an elegant solution to rendering the subject's appearance.

Parameterized face models can be learned across users leading to generic models, or within a subject creating a person-specific (PS) model. Generic models typically achieve robustness to lighting or user variability. However, these generic models do not provide accurate reconstruction for new subjects resulting in a loss of facial expression detail, making them not suitable for our scenario of interest. On the other hand, PS models can achieve the necessary accuracy in tracking and reconstruction. For these reasons, the PS model is typically used in the movie industry (e.g., The curious case of Benjamin Button). However, these models are typically run off-line and not perform well in untrained situations (e.g., different lighting). In this work, we present a lightweight process for specializing a personalized face model to new environments that enables extremely accurate real-time face tracking anywhere.

Our system performs a robust and efficient recovery of rigid and non-rigid motion from sequences with challenging illumination conditions using binocular video. It relies on a person-specific deep appearance model (PS-DAM) [Lombardi et al. 2018], which is learned in a multi-camera capture stage with fixed illumination. Although PS-DAM can generate high fidelity face renderings in real-time, accurately estimating its parameters in unconstrained settings remains challenging due to differences in illumination conditions and facial changes (e.g., facial hair, makeup, glasses). Finally, the entire system, including inference and rendering, needs to work in real-time to support interactive applications such as telepresence.

Our method has two main steps; learning and fine-tuning. In the first step (off-line face estimation in Fig. 1 left), we record several videos of a user and register their face using analysis-by-synthesis [Yuille and Kersten 2006]. In order to compensate for illumination changes and other factors, we introduce a parameterized *illumination model* and employ a "coarse-to-fine" fitting strategy to simultaneously estimate its parameters along with those of the face model, to avoid converging to poor local minima effectively. We use the resulting pairs of images and parameters to learn a real-time direct regression model. In the second step, we apply this regression model to estimate 3D shape and texture in real-time for a new environment. To compensate for differences between this environment and the environment where the regressor was trained in, we employ few-shot learning domain-adaptation [Zakharov et al. 2019] which fine-tunes our model from only a few images completely unsupervised. Our results show the effectiveness of this approach for driving a hyper-realistic 3D face model in unconstrained scenarios compared with competing state-of-the-art techniques (see Fig. 1 right).

In summary, this paper makes the following contributions:

- A real-time system for high-fidelity facial animation from binocular video. The system can track subtle expressions in uncontrolled environments (i.e., varying lighting).
- An neural illumination model to compensate from the domain mismatch between the face model and in-the-wild image. We use a coarse-to-fine fitting strategy to achieve better visual minima.
- A few-shot learning approach to fine-tune the pre-trained regression (encoder) to a new environment, in an unsupervised manner.

2 RELATED WORK

Research on face tracking and facial animation has a long history in computer vision, graphics and machine learning [Klehm et al. 2015; Zollhöfer et al. 2018]. In the following, we focus on the most related techniques and categorize the prior work into *parametric face modeling*, *real-time face tracking*, *lighting adaptation for face tracking*, and *non-parametric avatar animation*.

2.1 Parametric face modeling

Active Appearance Models (AAMs) [Cootes et al. 2001; Jing Xiao et al. 2004; Matthews and Baker 2004; Tzimiropoulos et al. 2013] and 3D morphable models (3DMM) [Blanz et al. 2003; Blanz and Vetter 1999] have been used extensively to model the space of facial appearance and geometry variation. This family of modeling methods is used to register faces using analysis-by-synthesis, and are often complemented with blendshape models to parameterize the space of expression variation [Lewis et al. 2014]. Extensions have focused on building multilinear models of identity and expression [Cao et al. 2013b; Vlasic et al. 2005], creating very large datasets to span the space of identity variation and texture [Booth et al. 2018], region-based models [Tena et al. 2011], joint shape and motion models [Li et al. 2017], and others [Gerig et al. 2018; Huber et al. 2016].

Recently, deep networks have been used to increase the modeling power of linear and multilinear models [Bagautdinov et al. 2018; Tran et al. 2019; Tran and Liu 2018]. In particular, [Lombardi et al. 2018] propose a Deep Active Appearance (DAM) model based on variational autoencoders [Kingma and Welling 2013] to capture photorealistic geometry and view-dependent appearance of human faces. In this work, we use the DAM model of [Lombardi et al. 2018]

to represent avatar appearance, and build an encoder suitable for real-time animation in unconstrained illumination.

2.2 Real-time face tracking

Real-time face tracking has been widely studied in the past decades [Zollhöfer et al. 2018]. Early real-time methods relied on tracking sparse facial features [Baltrušaitis et al. 2012; Chai et al. 2003; Saragih et al. 2011] as control signals for the face. Animation fidelity improvements have been achieved by increasing the tracking accuracy and density. For example, [Weise et al. 2011] used an RGBD sensor to build and track user-specific blendshape model and drive non-photorealistic avatars via expression retargeting. Subsequent work [Bouaziz et al. 2013; Chen et al. 2013; Li et al. 2013] using RGBD sensors showed that generic blendshape models can be adapted, corrected, or deformed to more accurately track a specific user.

In parallel, monocular RGB-only face tracking performance was improved by using data-driven regression of face landmarks or 3D shape [Cao et al. 2014, 2013a; Kazemi and Sullivan 2014; Xiong and De la Torre 2013] trained on large, annotated face datasets. This approach is robust to varying lighting conditions and unconstrained capture conditions. However, this robustness comes at cost to expression fidelity, and these models are still far from achieving the quality of offline facial performance capture.

To improve fidelity for face tracking, landmarks are also combined with dense appearance-based energies in optimization frameworks [Thies et al. 2016, 2018]. Appearance-based alignment via model fitting has a long history with AAMs and extensions [Jing Xiao et al. 2004; Kahraman et al. 2007; Matthews and Baker 2004], but building the AAM training set often requires capturing additional data in the target environment. Alternatively, [Cao et al. 2015] add face details by additionally regressing expression-dependent wrinkles. [Casas et al. 2015] use dynamic textures to improve photorealism, and [Nagano et al. 2018] improve realism by using a GAN network to synthesize dynamic textures from a single input image. [Cao et al. 2018] add optical flow constraints and a rigidity prior to stabilize the tracking.

Recent work in monocular face tracking has also explored direct regression of face model parameters using CNNs. For example, [Kim et al. 2017] use a large, synthetically generated set of images to train the CNN regressor. [Tran et al. 2017] use 3DMM fitting to generate the training data, while [Tewari et al. 2017] use differentiable rendering to train an image encoder that produces expression, albedo, and lighting parameters using self-supervision. Recent work on face tracking for VR headsets uses specialized training data generation methods, but also uses CNN-based regression of face parameters [Lombardi et al. 2018; Olszewski et al. 2016; Wei et al. 2019]. A related method to ours is that of [Laine et al. 2017], which achieves high-quality real-time face tracking using direct CNN image regression. There, the training data is built using an offline multiview face tracker, and tracking is limited to the lighting conditions and head pose observed in the capture stage. Our method combines sparse face landmark detection with a CNN-based face parameter regressor in texture-space to estimate detailed expression and pose parameters, and the realtime component is adaptable to novel lighting environments.

Real-time face tracking has also been used for photorealistic face reenactment [Thies et al. 2015, 2016, 2018], where only the face portion of a pre-recorded video is controllable. These techniques were later extended to provide upper-body control by using a 3D proxy [Thies et al. 2018] or using neural rendering to inpaint the areas surrounding the face [Kim et al. 2019, 2018]. While producing photorealistic results, these models can only produce a specific viewpoint and cannot be rendered from arbitrary directions.

2.3 Lighting adaptation for face trackers

Achieving dense, high-quality face tracking beyond coarse facial landmarks usually requires estimating or compensating for lighting conditions at evaluation time. Most existing face tracking methods use spherical harmonics (SH) lighting due to the speed and low degrees of freedom required to estimate them [Sengupta et al. 2018; Tewari et al. 2017; Thies et al. 2016]. [Valgaerts et al. 2012] estimate a spherical harmonics-based lighting environment for offline facial performance capture. [Fyffe et al. 2014] assume an HDR probe of the target environment is available, and use skin reflectance estimates from a light-stage capture to render and match using optical flow. [Yoon et al. 2019] achieve in-the-wild face tracking of a DAM model by training a regressor using self-supervised domain adaptation while ensuring temporal consistency. [McDonagh et al. 2016] train a person-specific regressor for facial performance capture to be robust to lighting changes by synthetically generating a large set of rendered images with varying synthetic lighting. In contrast, we learn from a small set of training sequences and use few-shot learning to adapt the regressor at test time.

2.4 Non-parametric Avatars

Non-parametric approaches rely on more sophisticated sensors to directly capture and transmit a 3D representation of the capture volume. Early realtime volumetric approaches, such as [Dou et al. 2017, 2016; Orts-Escolano et al. 2016], use several high-speed RGBD sensors to reconstruct and transmit full-body 3D avatar as meshes and textures. Progress in reducing the sensing requirements has been made by incorporating machine learning techniques to learn to fill holes produced by incomplete sensing or generate higher quality textures. In particular, [Martin-Brualla et al. 2018] showed full-body reconstructions with 16 active stereo cameras, and upper body reconstructions using a single stereo pair. This method uses a set of training views to learn a neural re-renderer that takes as input partial depth reconstructions and renders higher quality images. This was extended in [Pandey et al. 2019] to allow for full body volumetric capture using a single RGBD sensor, but requires several additional viewpoints during training for viewpoint generalization.

3 OVERVIEW

In this section, we introduce the hardware we are using to capture data (§ 3.1), and provide an overview of our algorithm in § 3.2.

3.1 Hardware and data capture

Hardware Setup. All of the data used in this work was collected using the setup depicted in Fig. 2 (a). The setup consists of a custom binocular webcam, which we refer to as *Facestar*, used to capture video, a desktop mount for the device, and a PC with custom capture software to record frames from the Facestar.

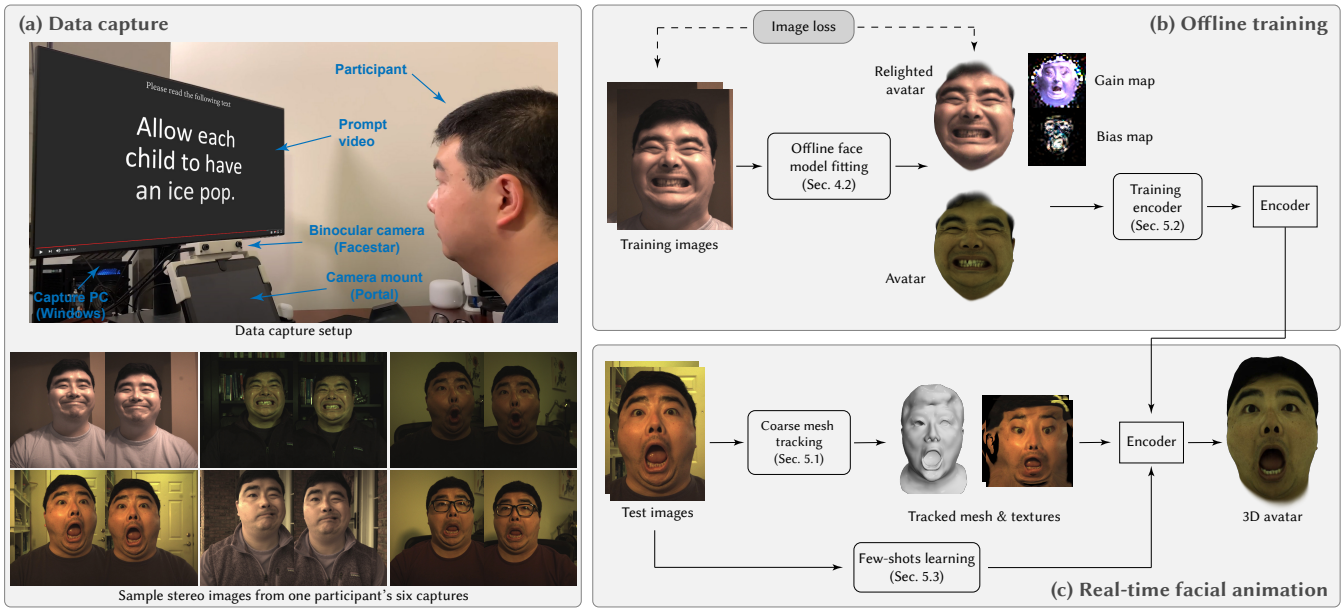

Fig. 2. Overview of our method. We use the binocular camera Facestar to capture user's facial performance in different environments (a). We then fit the DAM to the captured images, to get the groundtruth face parameters for each frame, which are used to train the encoder (b). The pre-trained encoder then can be used to drive the avatar animation in real-time (c).

We use this custom binocular camera to have better control of the camera settings, such as exposure time, white balance, resolution etc. The Facestar device (Fig. 3) has 2x OmniVision OV2312 cameras with a 100 mm baseline. The selected f/2.0 lenses provide a 35 degree and 43 degree HFOV and VFOV respectively. The lenses were focused to approximately 0.5m away, which was empirically determined to be a common desktop-mount distance for our participants. A custom camera controller is used inside the Facestar to simultaneously capture 2 MP (1300 x 1600) images from both RGB-IR cameras at 60 FPS and send them to the connected PC over USB 3.0. Custom software on the PC is used to perform debayering of the RGB pixels; the IR channel is discarded. The debayered images are encoded into a video using OpenCV. When necessary, single channel audio was recorded separately using a cell phone, using the built-in camera application.

Fig. 3. Facestar

Data Capture Procedure. Each participant was asked to capture themselves six times, ideally using two different lighting configurations in each of three different backgrounds. It was recommended that each participant simply rotate the Facestar twice, in 90 degree increments, to obtain 3 different backgrounds, and modify the lighting configuration by turning lamps on or off on either side of their face, though participants could choose other configurations if they were more convenient. One frame from each of the six captures for a participant is shown in Fig. 2 (a). At each frame we can get a pair of images $\{I^v\}_{v\in[0,1]}$. Each capture lasted about 8 minutes, during which the participant would follow along with a video showing a variety of facial expressions and sentences to read aloud, similar to the procedure in [Lombardi et al. 2018].

3.2 Algorithm overview

Fig. 2 (b)(c) shows the overview of our algorithm that has two stages. First, given a PS-DAM learned from a multi-camera system [Lombardi et al. 2018], an off-line analysis-by-synthesis method is applied on each frame to estimate accurate rigid and non-rigid face parameters in novel lighting environments (§4.2). The pairs of images and face parameters are used as training data to train an encoder for real-time inference (§ 5.2). Second, in the real-time facial animation stage, we take a user's new input video and combine a coarse mesh tracking algorithm (§5.1) with the encoder obtained from the off-line training step to achieve pixel-precise facial animation in real-time. The environments and lighting of the testing scenario may be different from those in the training data. To accurately recover the facial motions of testing images with new environments and lighting, we apply a few-shot learning strategy to adapt the encoder to the test images (§ 5.3).

4 FACE ESTIMATION

Our approach assumes the availability of a pre-trained person-specific parametric face model of mesh and appearance (PS-DAM). Given this model, this section describes how to produce realistic avatar animation by fitting the model to a binocular video with unmatched lighting conditions. Fig. 4 shows the overview of our proposed face estimation method.

4.1 Illumination Invariant Face Model

Given an input image pair, $\{I^v\}$, our goal is to estimate the full state of the face, comprising the rigid head pose and facial expression parameters. In this work, we use the Deep Appearance Model (DAM) proposed by [Lombardi et al. 2018] as the parametric face model. DAM generates mesh and view-dependent texture as a function of

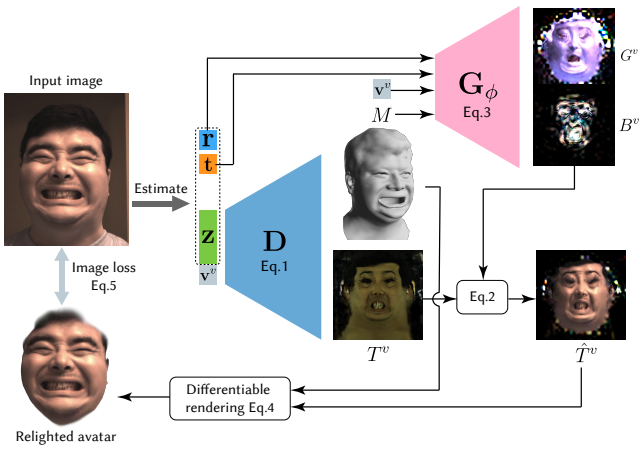

Fig. 4. Overview of offline face estimation. Given an input image, we estimate the rigid head pose $[\mathbf{r}, \mathbf{t}]$ and expression code $\mathbf{z}$. $\mathbf{z}$ and camera viewpoint vector $\mathbf{v}^v$ are fed into DAM to extract face mesh and texture. The head pose, viewpoint vector and face mesh are taken as input to the lighting model $\mathbf{G}_\phi$ to generate gain map G^v and bias map B^v, which are used to relight the texture. The face mesh M and relighted texture $\hat{T}^v$ are then rendered into the original image space to get a relighted avatar. We minimize the image loss between this relighted avatar and the input image.

a facial expression code $\mathbf{z} \in \mathbb{R}^{256}$:

$$M, T^v \leftarrow \mathbf{D}\left(\mathbf{z}, \mathbf{v}^v\right). \tag{1}$$

Here, $M \in \mathbb{R}^{n\times 3}$ is the face mesh comprising n-vertices and $T^v \in \mathbb{R}^{3\times w\times h}$ is the face texture with 3 channels (RGB). The viewing direction, $\mathbf{v}^v$, is the vector pointing from the center of the head to the camera v, and is used to account for view-dependent appearance variations such as specularities and texture changes due to imprecise mesh geometry. Because the face model that defines facial animation parameters is built in a capture stage with uniform lighting, its appearance does not typically span the lighting conditions in $\{I^v\}$, captured in unconstrained settings.

To compensate for these illumination differences, we build on recent work in domain transfer, and augment DAM with a color transformation applied to the texture T^v:

$$\hat{T}^v = T^v \odot G^v + B^v, \tag{2}$$

where $G^v \in \mathbb{R}^{3\times w\times h}$ and $B^v \in \mathbb{R}^{3\times w\times h}$ are gain and bias maps, and $\odot$ is the element-wise product operator, $\hat{T}^v$ is the relighted texture. To fully describe the appearance effects brought by illumination differences, these gain and bias maps depend on the specific illumination condition, rigid head pose, facial expression and viewing direction. Thus, we parameterize these maps using a neural network, that takes rigid head pose $[\mathbf{r}, \mathbf{t}]$, the face mesh M and camera viewpoint vector $\mathbf{v}^v$ as input:

$$G^v, B^v \leftarrow \mathbf{G}_\phi\left(\mathbf{r}, \mathbf{t}, M, \mathbf{v}^v\right), \tag{3}$$

where ϕ are the network parameters, and $\mathbf{r} \in \mathbb{R}^3$, $\mathbf{t} \in \mathbb{R}^3$ are the head rotation and the translation respectively. This construction, assumes that the illumination conditions are fixed during a capture session and that the camera is not moving in the environment.

To adapt to new environments, the lighting model, $\mathbf{G}_\phi$, is learned from scratch for every new environment from a small collection of calibration frames. This is performed jointly with the registration process to infer the face parameters in those frames as described in the §4.2. Given the capacity of the illumination model, the neural network can easily overfit to these frames and exhibit *cheating* behavior, where the lighting model also compensates for miss-registration instead of illumination effects only. This phenomenon has been observed previously in other works that use neural networks for domain adaptation [Schwartz et al. 2020; Wei et al. 2019]. In our work, we found that simply restricting the resolution of the network outputs and using the coarse mesh as input, instead of the full expression code, largely avoids overfitting when sufficiently good initialization is provided, as described next.

4.2 Off-line Face Model fitting

Given the rigid head pose $[\mathbf{r}, \mathbf{t}]$, the generated mesh M and transformed texture $\hat{T}^v$, we can project the face mesh to the original image space using the intrinsic camera parameters Π_v, and rasterize it to render a relighted avatar:

$$\begin{aligned} M^v &= \mathcal{P}\left(M, \mathbf{r}, \mathbf{t} \mid \Pi_v\right), \\ \hat{I}^v &= \mathcal{R}\left(M^v, \hat{T}^v\right), \end{aligned} \tag{4}$$

where $\mathcal{P}_{\Pi_v}$ is the projection operator based on the camera intrinsic matrix Π_v, $\mathcal{R}$ is the rasterization operator and M^v is the projected face mesh in screen space. In this way we can render the relighted avatar $\hat{I}^v$ in the original image space, and formulate the analysis-by-synthesis image loss:

$$\mathcal{L}_{im}(\mathbf{p}, \phi) = \sum_v \left(\left\|I^v - \hat{I}^v\right\|_1 + \lambda_{lap}\left\|\Delta I^v - \Delta \hat{I}^v\right\|_1\right), \tag{5}$$

where $\mathbf{p} = [\mathbf{r}, \mathbf{t}, \mathbf{z}]$ corresponds to the vector of face parameters, Δ is the image Laplacian operator and λ_{lap} is the weight of image Laplacian loss, and we choose $\lambda_{lap} = 0.2$ in our experiments.

The previous cost function, Eq. 5, defines a non-linear optimization problem that is prone to local minima. To provide a good initialization for the optimization, for each input image I^v, we detect 96 2D face landmarks $\{L_k^v\}$, that correspond to face features such as mouth corner, nose tip or face contour. For each landmark, k, we can find its corresponding vertex index on the face mesh denoted as ℓ_k, and calculate the L_2 distance between 2D face landmark and its corresponding mesh vertex projection:

$$\mathcal{L}_{land}(\mathbf{p}) = \sum_{v,k}\left\|L_k^v - M_{\ell_k}^v\right\|^2, \tag{6}$$

where M^v is the projected face mesh in screen space calculated by Eq.4.

At each step during the optimization, given the current estimated face parameters $\mathbf{p}_c$ and a lighting model $\mathbf{G}_\phi$, we can render the relighted avatar as $\hat{I}_c^v$ using Eq. 4. We then calculate the dense optical flow between $\hat{I}_c^v$ and input image I^v, and map the dense optical flow to the projected mesh vertices M_c^v in screen space through bilinear interpolation, annotated by $D^v = \{\mathbf{d}_i^v\}$. We can formulate the optical flow loss as the L_2 distance between the current projection of the face mesh M^v and the flow-predicted location $M_c^v + D^v$:

$$\mathcal{L}_{flow}(\mathbf{p}) = \sum_v \left\|M^v - M_c^v - D^v\right\|^2. \tag{7}$$

With these formulated losses Eq. 5 - 7, we can optimize the face parameters of all frames and the lighting model parameters by

Algorithm 1 Off-line face model fitting

Input: captured images $\{I^v\}$, detected 2D face landmarks $\{L_k^v\}$, intrinsic camera parameters Π_v.
Output: face parameters $\mathbf{p} = [\mathbf{r}, \mathbf{t}, \mathbf{z}]$, network parameters ϕ of the lighting model $\mathbf{G}_\phi$.
Process:

- **Step 1:** $\mathbf{p} \leftarrow \arg\min_{\mathbf{p}} \mathcal{L}_{land}$
- **Step 2:** Fix $\mathbf{p}$, then: $\phi_l \leftarrow \arg\min_{\phi} \mathcal{L}_{im}$
- **Step 3:** Calculate the optical flow, fix ϕ_l then:
  $$\mathbf{p} \leftarrow \arg\min_{\mathbf{p}} \mathcal{L}_{im} + \lambda_{land}\mathcal{L}_{land} + \lambda_{flow}\mathcal{L}_{flow}$$
- **Step 4:** Calculate the optical flow, then:
  $$\mathbf{p}, \phi_l \leftarrow \arg\min_{\mathbf{p},\phi_l} \mathcal{L}_{im} + \lambda_{land}\mathcal{L}_{land} + \lambda_{flow}\mathcal{L}_{flow}$$
- **Step 5:** Calculate the optical flow, fix ϕ_l, then:
  $$\mathbf{p}, \phi_h \leftarrow \arg\min_{\mathbf{p},\phi_h} \mathcal{L}_{im} + \lambda_{land}\mathcal{L}_{land} + \lambda_{flow}\mathcal{L}_{flow}$$

solving the following problem:

$$\min_{\{\mathbf{p}_t\},\phi} \sum_t \mathcal{L}_{im} + \lambda_{land}\mathcal{L}_{land} + \lambda_{flow}\mathcal{L}_{flow}, \tag{8}$$

where $\mathbf{p}_t$ is the face parameter vector at frame t. λ_{land} and λ_{flow} are used to control the weights of landmark loss and optical flow loss and are chosen as $\lambda_{land} = 1.0$ and $\lambda_{flow} = 3.0$ in our experiments. These optimized face parameters, are regarded as the groundtruth parameters in training the encoder for §5, and are denoted as $\mathbf{p}^\star = [\mathbf{r}^\star, \mathbf{t}^\star, \mathbf{z}^\star]$. The implementation details in solving the problem Eq. 8 will be discussed in §4.3.

4.3 Implementation details

Off-line fitting steps. We solve the optimization problem in Eq. 8 in several steps, which are listed in Algorithm 1. At Step 1, we only minimize the landmark loss formulated by Eq. 6 to obtain the face parameter $\mathbf{p}$ of each frame. Then we fix $\mathbf{p}$ and optimize the lighting model parameters at Step 2. We use a coarse-to-fine scheme to avoid overfitting. That is, we first optimize a low-resolution version of the lighting model parameters ϕ_l at this step, by minimizing the image loss described as Eq. 5. Then at Step 3, with the optimized $\mathbf{p}$ from Step 1 and ϕ_l from Step 2, we can render the relighted avatar $\hat{I}_c^v$ using Eq. 4, and calculate the dense optical flow between $\hat{I}_c^v$ and input image I^v. We then formulate the optical flow loss as Eq. 7. We fix the lighting model, and optimize the per-frame face parameters $\mathbf{p}$, by minimizing the image loss, landmark loss and optical flow loss. At Step 4, we jointly optimize ϕ_l and $\mathbf{p}$ to further minimize the loss. Finally, at Step 5, we fix the low-resolution lighting model's parameters ϕ_l, and jointly optimize $\mathbf{p}$ and high-resolution lighting model parameters ϕ_h, to refine the results. At Step 4 and Step 5, we similarly render the relighted avatar, calculate dense optical flow and formulate the optical flow loss.

Coarse-to-fine lighting model. Our lighting model is designed to describe the appearance effects brought by illumination differences between the DAM and the real data. However in practice, the lighting model can easily be overfitted to reconstruct the facial expressions from the captured images, which causes the "cheating" effects. For example, in Algorithm 1, as the estimated face parameters based on 2D face landmarks from Step 1 are not accurate, optimizing the lighting model in Step 2 can easily overfit the model to reconstruct the relighted avatar $\hat{I}^v$ matching input image I^v, but with wrong facial expressions. To mitigate this problem, we propose a coarse-to-fine lighting model, shown in Fig. 5. At Step 2, we only optimize the low-resolution lighting model $\mathbf{G}_{\phi_l}$, which outputs 32×32 gain and bias maps. We then up-sample them using bicubic interpolation to match the texture resolution, 1024×1024. The output low-resolution gian and bias maps help to avoid overfitting, and obtain accurate facial expression codes in Step 3 and Step 4. Then, at Step 5, given the current estimate of face parameters, we fix the low-resolution lighting model but optimize another high-resolution lighting model $\mathbf{G}_{\phi_h}$, which outputs a 256×256 gain and bias maps, to refine the details of the face. The experiments (Fig. 10) show that this coarse-to-fine lighting model helps to recover correct facial expression, while also reconstructing the captured lighting well.

5 REAL-TIME FACE ANIMATION

In the previous section, we proposed an offline method to fit a DAM model to arbitrary input video. In this section, we describe a direct regressor that allows real-time inference, based on the training data generated by the offline method. Fig. 6 shows the pipeline for real-time face animation. We first run a coarse mesh tracking algorithm on the input images (§5.1). These tracked meshes, and the unwarped textures are taken as input of an encoder to regress the target face parameters (§5.2). The regressed expression code, together with the camera view vector, are fed into the DAM to extract the face mesh and texture. Finally, the mesh, texture and rigid head pose are used to render the 3D avatar. In order to compensate for different illuminations in test videos, we use a few-shot learning strategy to adapt our pre-trained encoder (§5.3).

5.1 Coarse mesh tracking

To enable a real-time coarse mesh tracking, we build a linear PCA (Principal Components Analysis) model based on the tracked meshes from [Lombardi et al. 2018], annotated by $\{\bar{A}, A_1, A_2, ..., A_m\}$, where $\bar{A}$ is the average face and $A_1, A_2, ..., A_m$ are the principal components basis. Denoting a PCA coefficient vector as $\mathbf{a} = \{a_1, a_2, ..., a_m\}$ we can generate coarse face mesh as the linear combination of the PCA basis: $\mathcal{M} = \bar{A} + \sum_j a_j A_j$.

At each frame, for each image I^v from Facestar, we firstly detect 2D face landmarks $\{L_k^v\}$ using a real-time generic detector [Xiong and De la Torre 2013]. Similar to the landmark loss defined in Eq. 6, we can transform the face mesh $\mathcal{M}$ using rigid head pose $[\mathbf{r}, \mathbf{t}]$ and project it to image space using the camera intrinsic matrix Π_v, and penalize the L_2 distance between the 2D landmarks and their corresponding mesh vertices' projection:

$$\begin{aligned} \mathcal{M}^v &= \mathcal{P}\left(\mathcal{M}, \mathbf{r}, \mathbf{t} \mid \Pi_v\right), \\ \mathcal{L}_{track}(\mathbf{r}, \mathbf{t}, \mathbf{a}) &= \sum_{v,k} \left\| L_k^v - \mathcal{M}_{\ell_k}^v \right\|^2 . \end{aligned} \tag{9}$$

We use non-linear least squares minimization following [Cao et al. 2018] to optimize $\mathcal{L}_{track}$, and obtain the coarse mesh parameters $[\mathbf{r}, \mathbf{t}, \mathbf{a}]$ of each frame. We implement the optimization using the Ceres solver [Agarwal et al. 2010] to achieve the real-time performance at runtime.

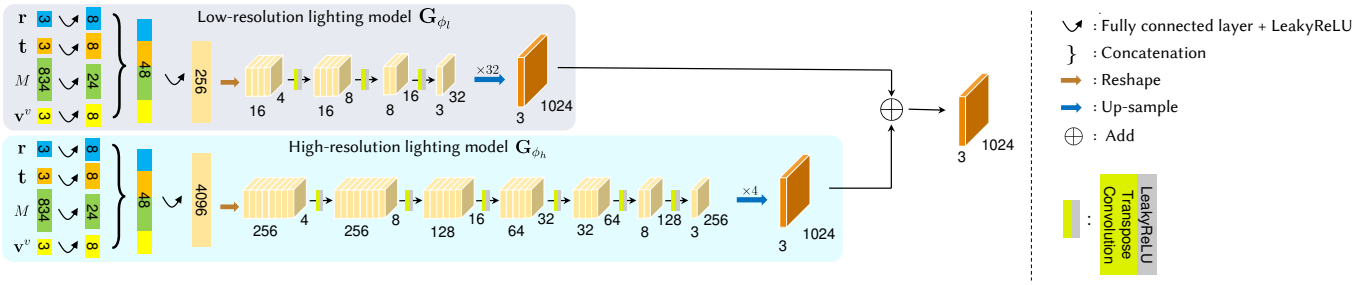

Fig. 5. Network architecture of the lighting model $\mathbf{G}_\phi$. We use a coarse-to-fine structure. The low-resolution lighting model (upper branch) outputs a 32×32 map, which is then up-sampled to 1024×1024. The lower branch, high-resolution lighting model outputs 256×256 map, which is up-sampled to 1024×1024 and added to output of the upper branch, to produce the final map.

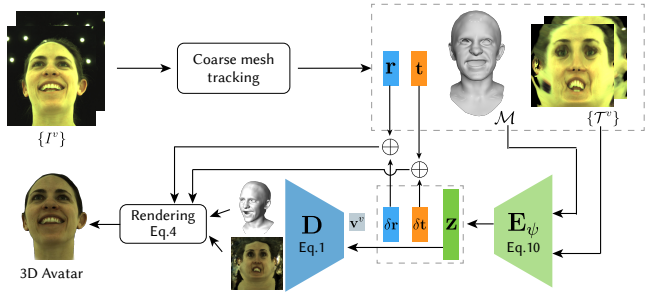

Fig. 6. The pipeline of real-time face animation. With input image pair $\{I^v\}$, we first run coarse mesh tracking to obtain the head pose $[\mathbf{r}, \mathbf{t}]$ and coarse mesh $\mathcal{M}$, which are used to unwarp texture $\{\mathcal{T}^v\}$. $\mathcal{M}$ and $\{\mathcal{T}^v\}$ are then fed into the encoder, to regress the head pose increments $[\delta\mathbf{r}, \delta\mathbf{t}]$ and expression code $\mathbf{z}$. $\mathbf{z}$ and the camera viewpoint vector $\mathbf{v}^v$ are taken as input of DAM to extract face mesh and texture. Finally, we add the increments to the initial rigid head pose estimates, and render the 3D avatar.

5.2 Encoder training

For each input image pair $\{I^v\}$, with the tracked coarse mesh from §5.1 and the corresponding groundtruth face parameters $\mathbf{p}^\star$ from §4.2, we can now train an encoder.

We firstly unwarp the input image I^v into the texture space with the projected coarse mesh $\mathcal{M}^v$, to get the captured textures $\mathcal{T}^v$. We then define the encoder, which takes the coarse mesh $\mathcal{M}$ and unwarped texture $\{\mathcal{T}^v\}$ as input, and outputs the expression code and rigid head pose increments:

$$\delta\mathbf{r}, \delta\mathbf{t}, \mathbf{z} \leftarrow \mathbf{E}_\psi\left(\mathcal{M}, \{\mathcal{T}^v\}\right), \tag{10}$$

where ψ are the network parameters of the encoder. The rigid head pose increments are simply applied to the estimated head pose from coarse mesh tracking: $\mathbf{r} + \delta\mathbf{r}$, $\mathbf{t} + \delta\mathbf{t}$. We expect these refined head pose and regressed expression codes to match the groundtruth parameters, thus we define a parameter loss by calculating the L_2 distance between the regressed results and the groundtruth:

$$\mathcal{L}_{param}(\psi) = \lambda_\mathbf{r}\|\mathbf{r}+\delta\mathbf{r}-\mathbf{r}^\star\|^2 + \lambda_\mathbf{t}\|\mathbf{t}+\delta\mathbf{t}-\mathbf{t}^\star\|^2 + \lambda_\mathbf{z}\|\mathbf{z}-\mathbf{z}^\star\|^2, \tag{11}$$

where $\lambda_\mathbf{r}$, $\lambda_\mathbf{t}$ and $\lambda_\mathbf{z}$ are weights to balance the units of rotation, translation and expression code, and we choose $\lambda_\mathbf{r} = 1e^3$, $\lambda_\mathbf{t} = 1e^{-2}$ and $\lambda_\mathbf{z} = 10$ in our experiments.

Additionally, with the regressed face parameters and the lighting model $\mathbf{G}_\phi$ obtained from §4.2, we can render the relighted avatar into the images based on Eq. 1-4, and define a loss directly in image space as Eq. 5. In our experiments, we firstly optimize ψ with 200 epochs by minimizing the parameter loss Eq. 11, and then further optimize ψ with 50 epochs by minimizing the image loss Eq. 5.

5.3 Few-shots learning adaptation

The environments and the lighting of the test scenarios may be different from the one of training data, thus directly applying the pre-trained encoder to data from new environments may lead to biased results. This section describes a few-shot learning strategy to adapt the encoder to new environments.

Fig. 7 shows the network architecture of the encoder, which consists of three branches. The first branch is a mesh branch, which takes the coarse mesh $\mathcal{M}$ as input. We sample 274 vertices from mesh $\mathcal{M}$ and construct a position vector using the 3D locations of these vertices, which is transformed using several fully-connected layers to get the latent vector. The second branch is a texture branch, which takes the unwarped textures $\{\mathcal{T}^v\}$ as input, down-samples it to 256×256, and encodes it using seven convolutional layers, with each layer followed by a BlurPooling layer [Zhang 2019]. The output is reshaped to a 4096 dimensional vector, and passed to several fully-connected layers to get a latent vector. This vector is concatenated with the latent vector from the mesh branch, from which the expression code $\mathbf{z}$ is regressed. Rigid head pose increments $\delta\mathbf{r}$ and $\delta\mathbf{t}$ are similarly regressed from the texture branch. To allow for few-shot learning of new environments in the encoder, inspired by [Zakharov et al. 2019], we add an embedder branch. The embedder branch also takes unwarped textures $\{\mathcal{T}^v\}$ as input. We use similar convolution layers in the texture branch, followed by two fully-connected layers to get adaptive parameters $\{\mu, \sigma\}$, which are applied to adaptive instance normalization layers in the texture branch. In general, we aim to learn the embedder branch such that the output vector $\{\mu, \sigma\}$ contains the video specific lighting information.

At runtime, with input test video of a novel lighting environment, we first uniformly sample K frames from the first 30 seconds of the test video. We use the off-line face estimation methods described in §4.2 to estimate the face parameters for these frames. To prevent the lighting model G_ϕ from overfitting on these limited frames, we select a pre-trained lighting model trained on one of this user's training video, and fine-tune it in Step 2 and Step 5 in Algorithm 1, instead of starting from scratch. We then define the parameter loss as Eq. 11 and image loss as Eq. 5, and adapt the pre-trained encoder. Experiments show that after 50 epochs, the adapted encoder can work well on the remaining frames of the test video.

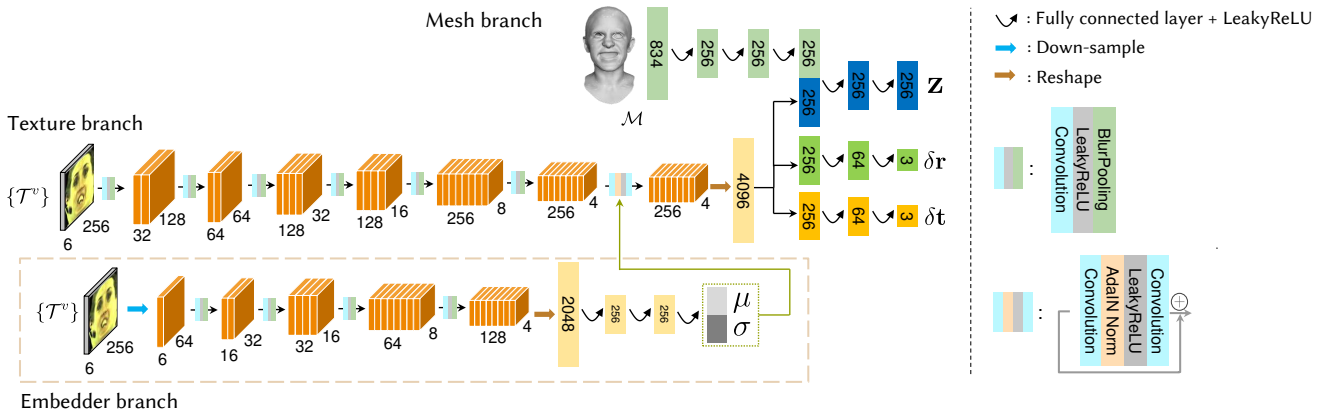

Fig. 7. The network architecture of encoder. We have three branches in encoder. From top to bottom: mesh branch, texture branch and embedder branch. The output of embedder branch, μ and σ are used as parameters for the adaptive instance normalization (AdaIn Norm) in the last convolution layer in texture branch.

6 RESULTS

In this section we describe the experiment setup and the timing of the system in §6.1, and presents a qualitative evaluation of the off-line face model fitting and real-time facial animation in§6.2. §6.3 describes an ablation study on different components of our algorithms. Finally, we compare our methods with state-of-the-art methods in §6.4.

6.1 Experiment setup

To build a user's PS-DAM, following [Lombardi et al. 2018], we use a large multi-camera capture apparatus which contains 40 machine vision cameras synchronously capturing images at 1334 × 2048 / 90 fps, and 460 white LED lights to promote uniform illumination. The user is asked to make a predefined set of 122 facial expressions and recites a set of 50 phonetically balanced sentences. This whole capture process takes about 1 hour to complete.

Facestar is then used to capture user's facial performance under six different in-the-wild environmental conditions. In each capture the user is asked to follow a video demonstrating a variety of facial expressions and sentences to recite. Each capture takes about 8 minutes to complete, for a total recording time of 48 minutes.

We then build PS-DAM based on the captured data in the multi-camera apparatus and estimate the face parameters in each Facestar captured video. We used the parameters of four video sequences for training the encoder. The entire preprocessing step takes about 3 days to finish on a GPU cluster. Once the PS-DAM and encoder are trained, a short sequence (less than 30 seconds) of the user's face performance is collected in a new target environment, which is used to fine-tune the encoder. In under 1 hour processing on 4 GPUs (Table 3) the user can drive her/his avatar in real-time in the new target environment.

6.2 Qualitative Evaluation

We used Facestar to capture seven users' facial performance under six different environmental conditions (42 videos in total). For each video sequence, we estimate the face parameters using the method described in §4.2, that provides our ground-truth. We then used the parameters of four video sequences of an user as training data to train the encoder, and the remaining two videos for testing.

Off-line face model fitting . Fig. 1 and Fig. 17 shows the offline face model fitting on different users under different environments. Our method can estimate accurate face parameters, including the rigid head pose and non-rigid facial expression code, which can animate the avatar (b) with the same facial expression as the input image (a), demonstrating the quality of the facial expression transfer, including eyelids, gaze, lip shape, wrinkles, teeth and tongue. Our proposed lighting model effectively generates gain and bias maps (e) which models the illumination changes due to different lighting conditions, head pose and facial expressions, which help to relight the avatar (b) to pixel-wise match the input image. Though the PS-DAM does not model glasses, our methods can still handle the case with glasses on (Fig. 17 3rd row), by encoding the glasses into the gain and bias map.

Our method can also be applied to other consumer RGBD cameras (i.e. Intel RealSense, iPhoneXS etc.) to achieve a fitted face model with similar quality as with using Facestar. In Fig. 8 we show the results of estimating the face parameters from RGBD images from an iPhoneXS. Besides the losses defined in Eq. 8, we also compute the L_1 error between the rendered depth map (Fig. 8 (g)) and captured depth map (Fig. 8 (f)), which helps to achieve stable rigid alignment in place of the multi-view images in Facestar.

Real-time facial animation . For each user, we took her/his four videos sequences to train the encoder (Fig. 7). The other two video sequences are used as test data. We uniformly sampled K frames from the first 30 seconds of the test videos, and adapt the encoder following a few-shot learning strategy described in §5.3. We then applied this adapted encoder to other frames of the test videos. The output of this process is shown in Fig. 1 and Fig. 18. With the input image from the binocular camera, each person can drive her/his own avatar to generate the photo-realistic avatar animation, covering wide range of facial motions. With the view-conditioned DAM representation [Lombardi et al. 2018], we can also visualize the 3D avatars from different views, which allows our methods to be

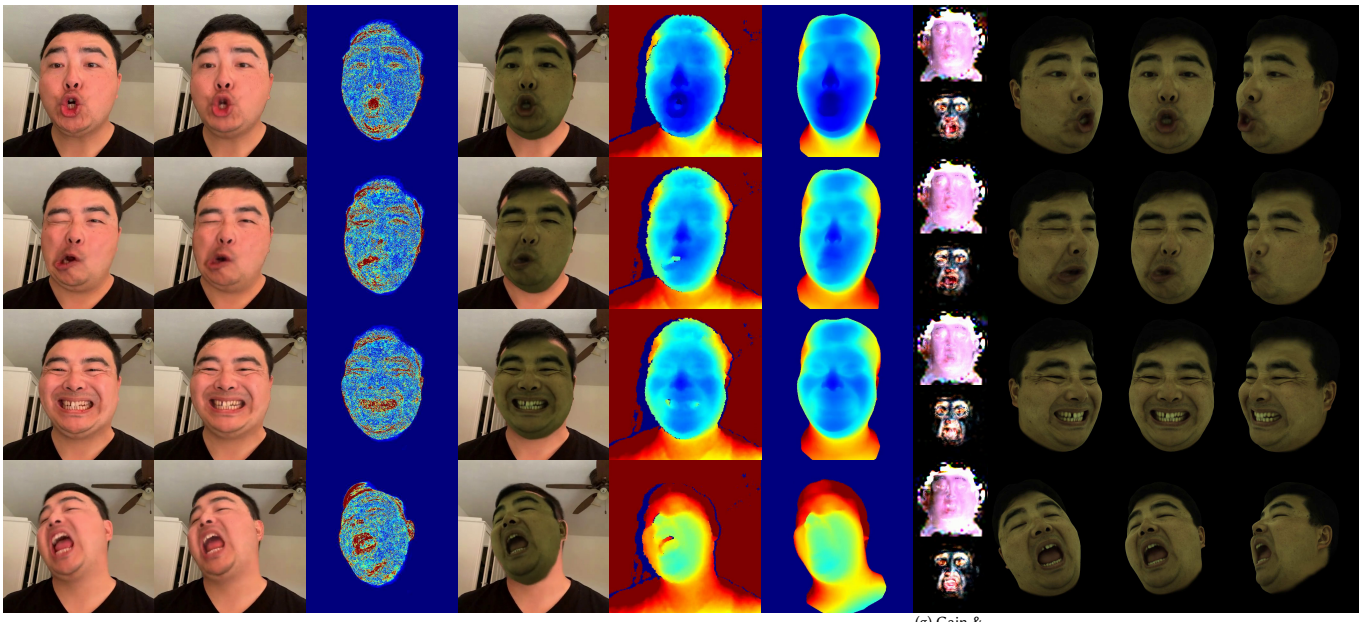

(a) Input image (b) Relighted avatar (c) Reconstruction error (d) Avatar (e) Input depth (f) Rendered depth (g) Gain & bias map (h) 3D avatar from different views

Fig. 8. Off-line face model fitting on iPhoneXS data. With input image (a) and depth (f) from iPhoneXS, our algorithm estimates accurate face parameters to animate the avatar with the closely matching facial expression and motion (b, d, g).

Fig. 9. Using a robust loss function without a lighting model in off-line face model fitting. From top to bottom: input images, fitted avatars using robust loss function without a lighting model, our fitted avatars.

used in AR/VR applications. We implemented the facial animation methods on a Windows machine with 64 cores CPU and 2 Nvidia GTX 2080 GPUs, which allows us to drive the avatar at 45 fps. Please see our supplementary video for a live demo.

6.3 Ablation Study

This section performs an ablation study of different components of the algorithms.

Robust loss function without a lighting model. We proposed a novel lighting model to fill the domain mismatch between DAM and in-the-wild video. Can we ignore this domain mismatch and define a robust loss function to fit the face model parameters directly? In this ablation study, we defined a domain-independent perceptual loss in addition to other losses defined in Eq. 5 - Eq. 7. We passed both the rendered avatar and input image into the VGG19 network ([Simonyan and Zisserman 2014]), got the output features, and calculated the L_1 loss of the corresponding features. Fig. 9 shows the results of face model fitting by optimizing these losses. While the perceptual loss help to recover the sematic expression to some extent, the facial motions of the fitted avatar (Fig. 9 middle row) have a clear gap to the input image (Fig. 9 top row). As a comparison, our method used the pixel-wise image loss, which can help to recover precise facial expressions (Fig. 9 bottom row).

Coarse-to-fine lighting models. The key component of the off-line face model fitting is the lighting model. A good lighting model is critical to recover the illumination differences between DAM and in-the-wild image, and have an accurate estimate of the face parameters. We choose a coarse-to-fine network architecture as the lighting model (Fig. 5), and compared with other architectures.

To get the ground-truth face parameters, we recorded facial performance data in a calibrated multi-view light-stage consisting of 40 vision cameras synchronously capturing images at 1334×2048 / 90 fps and a total of 460 white LED lights. We flash a group of LEDs (at most 10) at each frame, and turn on all LEDs every 3rd frame to get fully lit images. These full-lit images have the same lighting conditions as the DAM, so we can directly define the image loss without applying any lighting adaptation and get ground-truth face parameters on these full-lit images. These face parameters are then interpolated to in-between frames, to get the ground-truth face parameters for frames with non-uniform lighting conditions.

For testing, we choose frames with one particular lighting condition, and run our off-line face model fitting pipeline to fit the face parameters and reconstruct the input image. We will compare

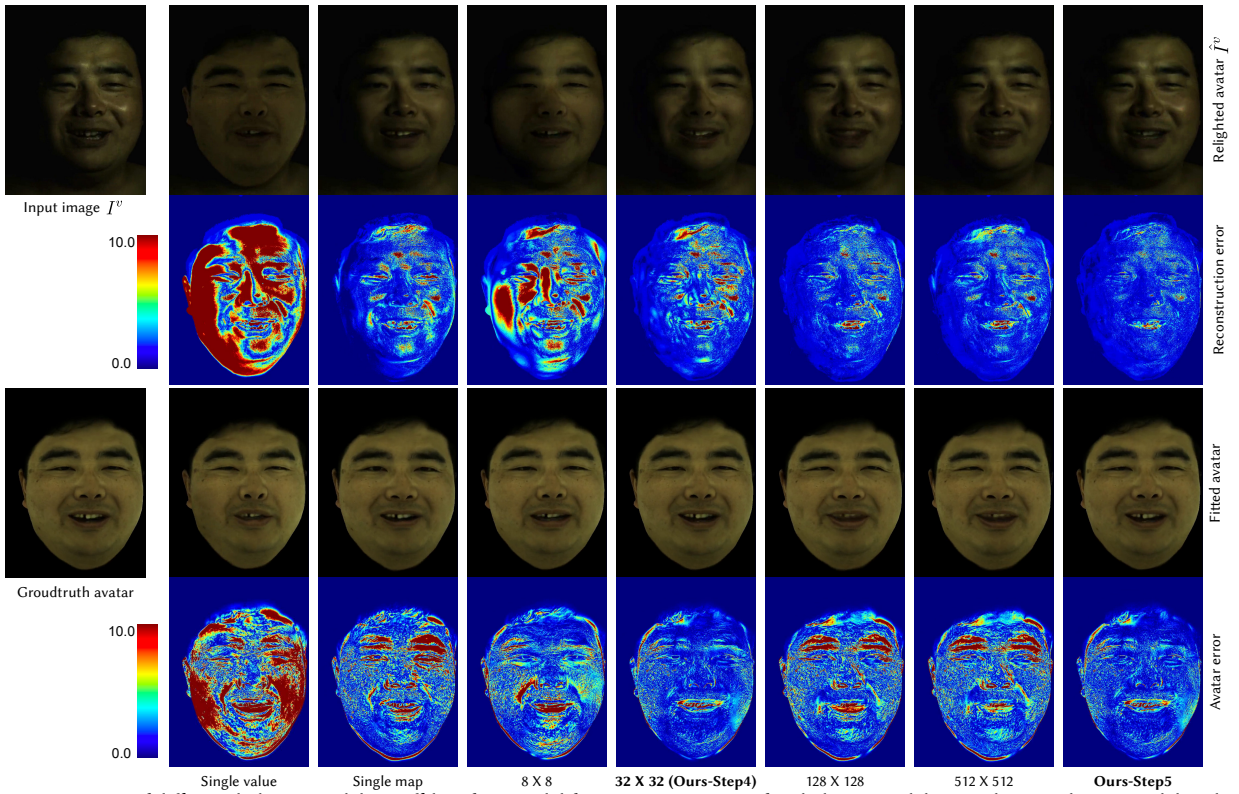

Fig. 10. Comparisons of different lighting models in off-line face model fitting. Our coarse-to-fine lighting model uses a low-resolution model with 32×32 output first, plus a high-resolution model with 256×256 output, which generates the most accurate avatar while gives the best reconstruction.

Table 1. Comparisons of off-line face model fitting using different lighting models.

Methods	Reconstruction Error	Avatar Error
Single value	7.79	10.00
Single map	3.01	7.90
8×8	3.91	5.08
32×32 (Ours-Step4)	**2.53**	**4.60**
128×128	2.09	6.04
512×512	2.21	7.83
Ours-Step5	**1.79**	**4.42**

the L_2 image loss between the relighted avatar and input image (*Reconstruction Error*), and the L_2 loss between the avatar rendered using estimated parameters, and the ground-truth rendered avatar (*Avatar Error*). This avatar loss reflects the accuracy of the fitted face parameters.

The simplest lighting model is a single gain and bias value. The lighting model takes rigid head pose, face mesh and camera viewpoint vector as input, outputs single gain and bias value, which are then expanded to the gain and bias maps (*Single value*). We also try to optimize a single, frame-independent gain and bias maps at 1024×1024 resolution (*Single map*). On the other hand, we tested lighting models similar to our low-resolution lighting model, but with different output resolution: 8×8, 128×128, 512×512. The output of these lighting models are up-sampled to 1024×1024 resolution.

Tab. 1 shows the errors using different lighting models in our pipeline, and Fig. 10 shows one example frame using different lighting models. The input face image has non-uniform lighting. Single gain/bias values are insufficient to model this lighting change, which results in both wrong reconstructed avatar (large avatar error) and poor reconstruction (large reconstruction error). The single map lighting model can lower the reconstruction loss as it has different gain/bias values at different pixels. However, as the lighting will change due to different head pose and facial expressions, single map cannot model the lighting variability across different frames. For lighting models with different output resolutions, the one with larger resolution (128×128 or 512×512) has too much capacity, which will get good reconstruction (smaller reconstruction errors), but it fails to estimate accurate face parameters, and results in wrong reconstructed avatar (large avatar error). We call this effect as *"Cheating"* effect. As a comparison, in our strategy, we first used a low-resolution lighting model with 32×32 resolution output, to estimate the face parameters in Step 2 - 4 of Algorithm 1. Then in Step 5, we add another high-resolution lighting model with 256×256 output, to refine the face details. Our coarse-to-fine lighting model gives the most accurate face parameters (lowest avatar error) and the best reconstruction (lowest reconstruction error).

Two views vs. single view. We used Facestar, the binocular cameras to simultaneously capture an image pair from two different views at each frame, which are taken as input in all our experiments in this paper. To evaluate the importance of these two views input,

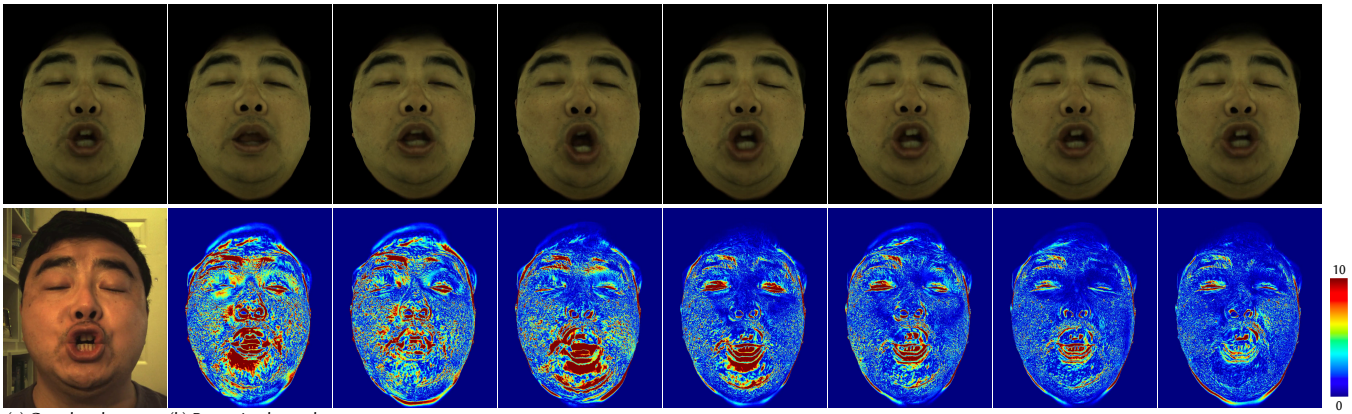

Fig. 11. Ablation study on few-shots adaptation. Directly apply the pre-trained encoder to the test video will fail in tracking accurate facial motions. With more frames from test video in adapting the encoder will help to get more accurate avatars, but brings more computation time. In our experiments, we find $K = 256$ can already give satisfying results.

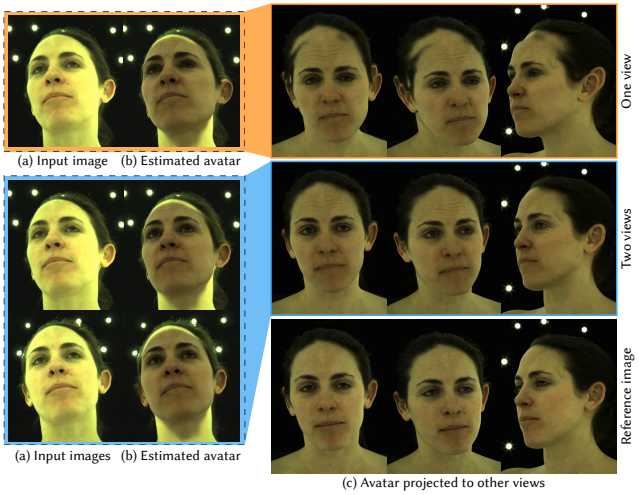

Fig. 12. Face model fitting with one view input and two views input. The estimated model has a clear offset from the face in reference image based on one view input due to the depth ambiguity, while two views input can resolve this.

we evaluated our method on single view input of Facestar. Fig. 12 shows the comparisons. We put a Facestar in the light-stage system with multiple cameras, which are calibrated with the two cameras of Facestar. We then trigger the Facestar camera and light-stage cameras at the same time to capture the synchronized face images. We took the image captured from Facestar's left camera as input, estimated the face model parameters using methods of §4.2, and projected the estimated avatar to other view images captured by light-stage cameras via the calibrated matrices. As shown in the top row of Fig. 12, though the estimated avatar aligns well in the input image, the projected avatar has a clear offset from the face in other view images. The reason is that the estimated depth from the single view input has a large ambiguity. Using two views from Facestar can help to resolve this ambiguity, and obtain the aligned avatar in other view images (Middle row of Fig. 12).

Table 2. Ablation study on using different lighting conditions in training data, and embedder branch.

Methods	Avatar Error	Decrease
2 lightings w/o embedder	5.24	NA
2 lightings	4.19	20.0%
4 lightings w/o embedder	3.16	NA
4 lightings	2.74	13.3%

Table 3. Using different numbers of frames to adapt the pre-trained encoder.

Methods	Avatar Error	Adaptation Time
Pre-trained encoder	4.19	NA
K = 64	3.11	4 mins
K = 128	2.92	8 mins
K = 256	2.78	15 mins
K = 512	2.69	31 mins
K = 1024	2.68	59 mins

Different lightings in training data. We used training data with different lighting conditions to train the encoders, and apply the encoder to test video with another lighting condition, and compute the L_2 avatar error. Tab. 2 shows the comparisons between two lighting conditions and four lighting conditions. As expected, the more variability that we have in the training data, in general, the better the model will be able to generalized.

Embedder branch in encoder. To evaluate the embedded branch in our encoder architecture, we removed the last convolution layer in the texture branch from the original encoder, and train it using the same training data. We then applied this encoder to another test video sequence and compared the L_2 avatar errors. Tab. 2 shows the comparisons with/without the embedded branch in the encoder. For the encoder trained using data with 2 lighting conditions, adding the embedded will help to decrease the avatar error by 20.0%, and 13.3% for the case with 4 lighting conditions. Fig. 11 (b)(c) show one example frame of animated avatar from the input image. Our encoder with the embedded branch (c) help to recover better mouth shape than the one without the embedded branch (b).

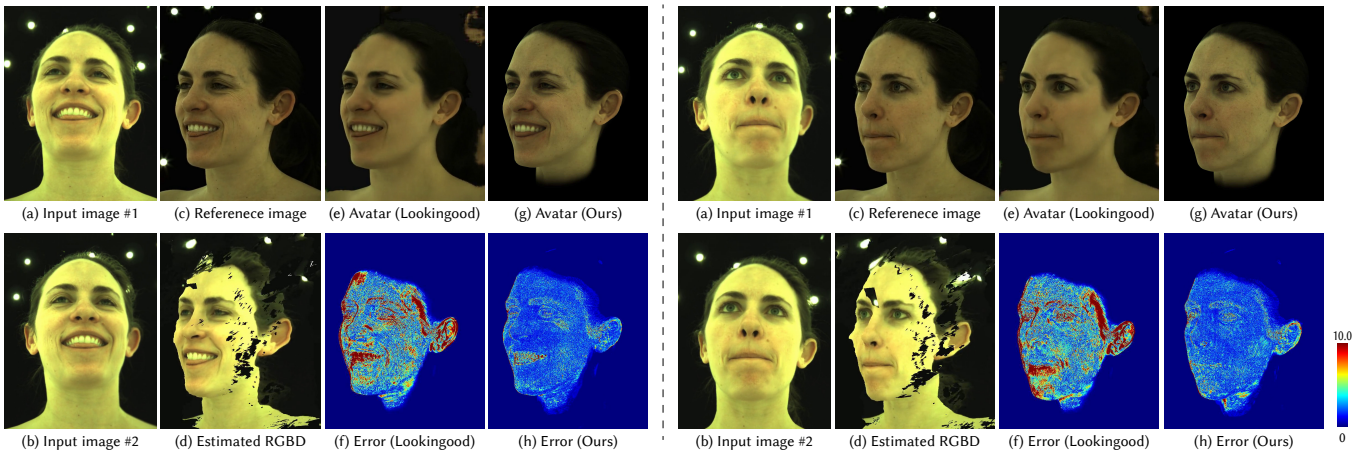

Fig. 13. Comparisons with Lookingood [Martin-Brualla et al. 2018] on data captured in light-stage. With input image pair (b) from Facestar, we estimate the depth using vision stereo algorithm, and construct the RGBD data (d). Lookingood takes this RGBD as input, infer the dense, complete volumetric avatar representation (e). Avatar generated by our method (g) contains more face details, and has lower reconstruction error (h) than Lookingood (f). Please notice that our methods only replies on the input images (a-b), not the RGBD input (d).

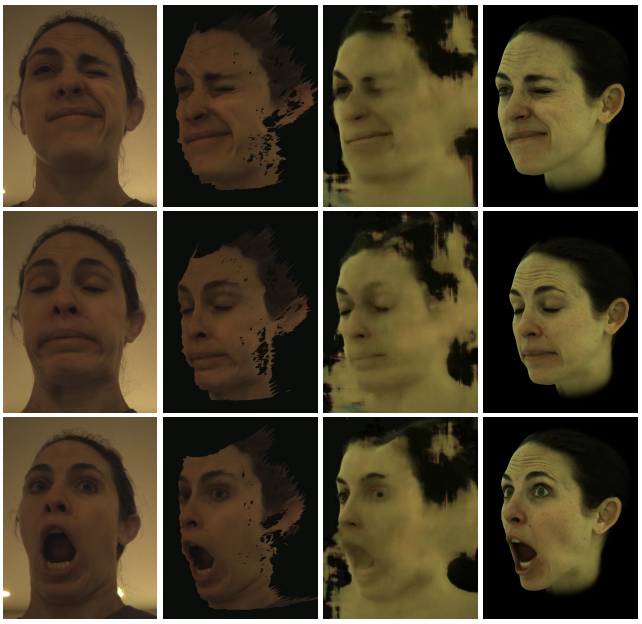

Fig. 14. Comparisons with Lookingood [Martin-Brualla et al. 2018] on in-the-wild video. The re-rendering network of Lookingood is trained on light-stage data, which can not be generalized well to in-the-wild video (c). Our method gives satisfying results (d) thanks to the proposed lighting model.

Selection of K in adapting the encoder. At runtime, the more frames we used from the test data to fine-tune the pre-trained encoder the better we are able to adapt the encoder to test video; however, the more frames we select the more expensive is the computation. To study the selection of K, we first used two videos of one user to train an encoder. Then we uniformly sample K frames from the first 30 seconds of the test video, estimated the face parameters using method from §4.2, and adapted the encoder. Finally, we applied the adapted encoder to other frames of the test video, and compared the L_2 avatar error to the ground-truth avatars. Tab. 3 shows the avatar errors and adaptation times with different K. When K is increased from 512 to 1024, the avatar errors are very close already. Fig. 11 shows one example frame which is not used to adapt the encoder. Though the error is decreased a little bit, but it is hard to tell the differences from the visual results after $K = 256$. Considering the performance, we choose $K = 256$ in all our experiments.

Table 4. Reconstruction error of Lookingood [Martin-Brualla et al. 2018] and our method on light-stage data.

Methods	Reconstruction Error
Lookingood	5.86
Ours	**2.65**

6.4 Comparisons

This section compares our methods with other state-of-the-art facial animation methods.

Non-parametric avatars. First, we compared our method to a recently non-parametric avatar method "Lookingood" [Martin-Brualla et al. 2018]. Their system takes real-time, low-quality RGBD data of user facial performance as input, which may suffer from artifacts such as holes and noise in the rendering, and use a deep architecture to perform completion, super resolution and denoising in real-time. To collect the training data to train this system, similar to what we do in ablation study, we put the Facestar in a light-stage containing multiple cameras, to capture user's facial performance from Facestar and light-stage cameras. The images captured by light-stage cameras are used to build a volumetric avatar of the user. With an input image pair from the Facestar, at each frame, we find the pixel correspondence between the paired images, and estimate the depth using vision stereo algorithm. Based on these data, we can train a machine learning framework called neural re-rendering, to infer the dense, complete volumetric representation (Fig. 13 (e)) from noisy, low-quality RGBD data (Fig. 13(d)). As a comparison, we used the images captured by light-stage cameras to build the DAM [Lombardi et al. 2018], and used our method to drive the avatar animation from Facestar images (Fig. 13(g)).

(a) Input image (b) [Cao et al. 2018] (c) Ours (a) Input image (b) [Cao et al. 2018] (c) Ours (a) Input image (b) [Cao et al. 2018] (c) Ours

Fig. 15. Comparisons with landmark and optical flow based face tracking methods [Cao et al. 2018]. The sparse landmark and optical flow are not able to describe the complete and subtle facial expressions, results in avatar missing many expression details.

Fig. 13 shows two example frames from the test video comparing Lookingood [Martin-Brualla et al. 2018] with our method. From the visual avatar results (e-g), both methods can reconstruct an accurate 3D avatar from input images (a-b). However, our results contain more facial details such as the face pores, while Lookingood gives over smoothed results. We take the image captured from one light-stage camera as the reference image, project the avatar into the image, and calculate the L_2 reconstruction error inside the face region, shown as (f-h). We can see our method produces lower reconstruction error. We calculated the reconstruction error on the whole video sequence with ~7K frames, and get the average reconstruction error shown as Table 4, which shows that our method can give lower reconstruction error than Lookingood.

Our proposed lighting model helps to fit the face model to data captured under different environments, so that we can not only reconstruct avatars for video captured inside the light-stage, but in-the-wild video. Fig. 14 shows examples of our method being applied to the in-the-wild input images (a), and reconstruct avatar with accurate rigid head pose and facial expressions (d). Directly applying the Looking-Good model, trained on light-stage data, on these in-the-wild image and the estimated RGBD data (b) cannot get satisfied results (c).

Real-time landmark-based facial animation. In recent years, markerless, real-time face tracking methods based on 2D images are widely explored and used in many gaming and AR applications. A major approach is to detect the 2D face landmarks, then use these 2D landmarks to track the 3D face. To enhance the temporal coherence and rigid stability, [Cao et al. 2018] also used optical flow as constraints during optimization. We extend their method to binocular cameras input, using 2D facial landmarks and optical flow as constraints to optimize the rigid head pose and expression code of DAM. Fig. 15 (b) shows several example frames. These sparse landmarks and optical flow are not able to describe complete and subtle facial expressions. While [Cao et al. 2018] can recover right expression in specific expressions with distinctive face geometry (Frame #3), their method cannot reconstruct correct expression for other frames, especially the details on eyes (Frame #1), teeth (Frame #2) and lip shape (Frame #3,#4) and gazes (Frame #6).

Table 5. Comparisons with [Yoon et al. 2019] and [Li et al. 2018]

Methods	Reconstruction Error
[Yoon et al. 2019]	6.81
[Li et al. 2018]	7.44
Ours	**2.69**

Other lighting adaptation for face tracking. We compared our method to other methods that use different lighting adaptation schemes for face tracking. [Yoon et al. 2019] proposed I2ZNet, which tracks the DAM by training a regressor using self-supervised domain adaptation. I2ZNet learns a single 1-by-1 convolution layer at the output texture of DAM as the color transformation, which helps to correct the white-balance between the two domains. We first trained the I2ZNet on the light-stage data which are used to construct DAM, and adapted the model on in-the-wild data in a self-supervised way. Fig. 16 (b) shows the results. Their proposed lighting adaptation model (i.e. the 1-by-1 convolution layer) fails when using challenging lighting conditions, which results in poor quality avatars with artifacts.

On the other hand, we also compared our method with the common lighting model used in previous work, spherical harmonics (SH). We replaced the lighting model with SH in our system. We followed the environment map prediction methods proposed by [Li et al. 2018], to train a network to predict the first nine SH coefficients for each color channel from the input texture. These SH coefficients, together with the normal map of face mesh extracted from DAM, are used to relight the face texture. We then render the relighted avatar using these relighted texture, and calculate the image loss between the relighted avatar with input image. This image loss can be minimized to obtain the optimal rigid head pose and expression code. Fig. 16 (c) shows the results. The SH lighting model can only recover the low-frequency lighting differences, thus the optimized avatar based on this lighting model contain mismatch facial details, such as blur mouth lip and wrong eye lids. Our methods can reconstruct an avatar with precise facial expressions, and get lower reconstruction error (Fig. 16(d)) thanks to our coarse-to-fine lighting model. Table 5 also shows the reconstruction error using different lighting adaptation methods, while our method can give the lowest reconstruction error.

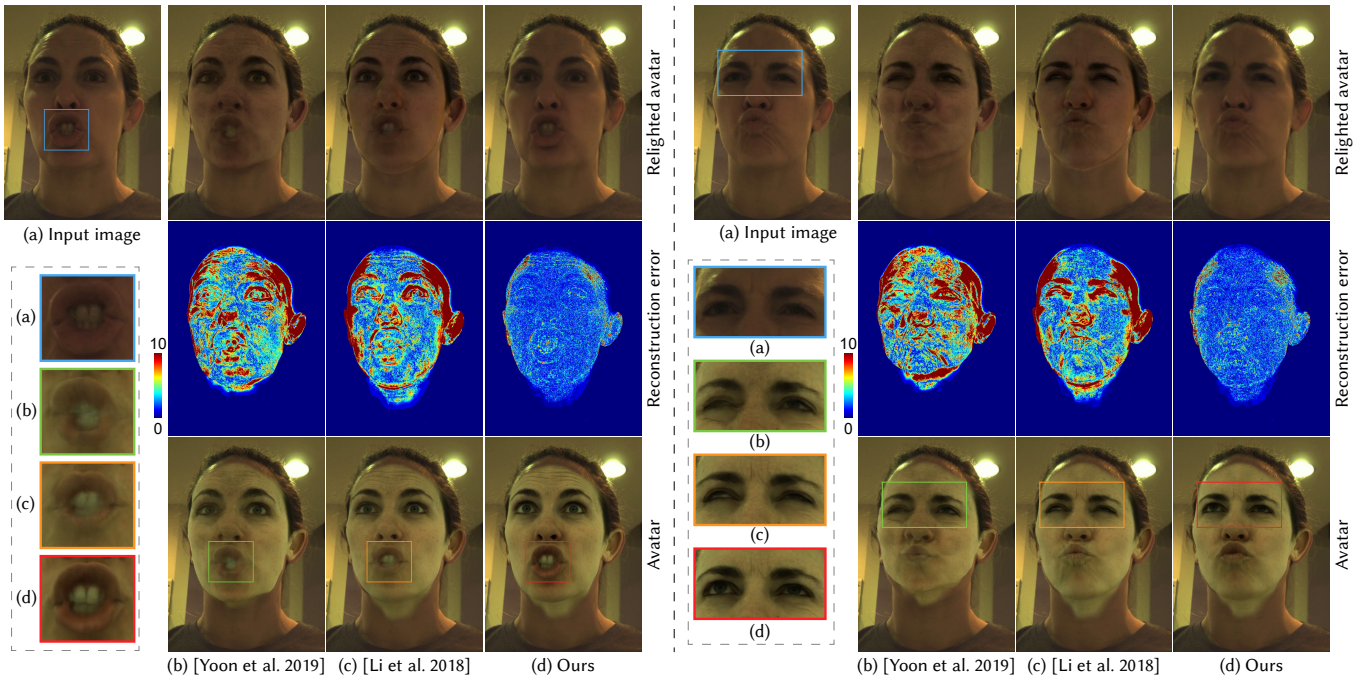

Fig. 16. Comparisons with [Yoon et al. 2019] and [Li et al. 2018]. Neither the 1-by-1 convolution layer from [Yoon et al. 2019] nor spherical harmonics from [Li et al. 2018] can describe the complex illumination difference, result in blur and inaccurate face details in reconstructed avatar. While our lighting model can model the lighting well, and gives satisfying avatar results.

7 CONCLUSION

We propose a real-time method to drive hyper-realistic avatars from a binocular RGB camera. Given the input video and a pre-trained DAM, we fit the face model to a video, decoupling the rigid head pose from facial expressions. We propose a novel coarse-to-fine lighting model to fill the domain gap between DAM and in-the-wild video with unconstrained lighting condition. To drive the high-fidelity avatar animation in real-time, we design a few-shot learning based regressor, which can be quickly adapted to test scenario by observing a few frames of new environments.

There exists some limitations of our method. First, we assume the lighting conditions during user's capture will not change dramatically, which is not true in some cases. In the future, we will explore an online adaptation strategy to adapt the encoder. Second, we now only model the face animation, but not the hair, neck or shoulder. We may extend our method to upper body animation in the future work. Finally, our method is still a person specific solution. To make our system more practical to users, we will explore a general method to drive the high-fidelity avatar animation.

REFERENCES

Sameer Agarwal, Keir Mierle, and Others. 2010. Ceres Solver. http://ceres-solver.org.

Timur Bagautdinov, Chenglei Wu, Jason Saragih, Pascal Fua, and Yaser Sheikh. 2018. Modeling Facial Geometry Using Compositional VAEs. In *Proceedings of the IEEE Conference on Computer Vision and Pattern Recognition (CVPR)*.

T. Baltrušaitis, P. Robinson, and L. Morency. 2012. 3D Constrained Local Model for rigid and non-rigid facial tracking. In *2012 IEEE Conference on Computer Vision and Pattern Recognition*. 2610–2617. https://doi.org/10.1109/CVPR.2012.6247980

Volker Blanz, Curzio Basso, Tomaso Poggio, and Thomas Vetter. 2003. Reanimating Faces in Images and Video. *Comput. Graph. Forum* 22 (09 2003), 641–650. https://doi.org/10.1111/1467-8659.t01-1-00712

Volker Blanz and Thomas Vetter. 1999. A morphable model for the synthesis of 3D faces. In *Proceedings of the 26th annual conference on Computer graphics and interactive techniques*. 187–194.

James Booth, Anastasios Roussos, Allan Ponniah, David Dunaway, and Stefanos Zafeiriou. 2018. Large scale 3D morphable models. *International Journal of Computer Vision* 126, 2-4 (2018), 233–254.

Sofien Bouaziz, Yangang Wang, and Mark Pauly. 2013. Online Modeling for Realtime Facial Animation. *ACM Transactions on Graphics (TOG)* 32, 4 (July 2013), 10.

Chen Cao, Derek Bradley, Kun Zhou, and Thabo Beeler. 2015. Real-Time High-Fidelity Facial Performance Capture. *ACM Trans. Graph.* 34, 4, Article 46 (July 2015), 9 pages. https://doi.org/10.1145/2766943

Chen Cao, Menglei Chai, Oliver Woodford, and Linjie Luo. 2018. Stabilized Real-Time Face Tracking via a Learned Dynamic Rigidity Prior. *ACM Trans. Graph.* 37, 6, Article 233 (Dec. 2018), 11 pages.

Chen Cao, Qiming Hou, and Kun Zhou. 2014. Displaced Dynamic Expression Regression for Real-time Facial Tracking and Animation. *ACM Transactions on Graphics (TOG)* 33, 4 (July 2014), 43:1–43:10.

Chen Cao, Yanlin Weng, Stephen Lin, and Kun Zhou. 2013a. 3D Shape Regression for Real-time Facial Animation. *ACM Transactions on Graphics (TOG)* 32, 4, Article 41 (July 2013), 10 pages.

Chen Cao, Yanlin Weng, Shun Zhou, Yiying Tong, and Kun Zhou. 2013b. Facewarehouse: A 3d facial expression database for visual computing. *IEEE Transactions on Visualization and Computer Graphics* 20, 3 (2013), 413–425.

Dan Casas, Oleg Alexander, Andrew W. Feng, Graham Fyffe, Ryosuke Ichikari, Paul Debevec, Rhuizhe Wang, Evan Suma, and Ari Shapiro. 2015. Rapid Photorealistic Blendshapes from Commodity RGB-D Sensors. In *Proceedings of the 19th Symposium on Interactive 3D Graphics and Games (i3D '15)*. Association for Computing Machinery, New York, NY, USA, 134. https://doi.org/10.1145/2699276.2721398

Jin-xiang Chai, Jing Xiao, and Jessica Hodgins. 2003. Vision-Based Control of 3D Facial Animation. In *Proceedings of the 2003 ACM SIGGRAPH/Eurographics Symposium on Computer Animation* (San Diego, California) *(SCA '03)*. Eurographics Association, Goslar, DEU, 193–206.

Y. Chen, H. Wu, F. Shi, X. Tong, and J. Chai. 2013. Accurate and Robust 3D Facial Capture Using a Single RGBD Camera. In *2013 IEEE International Conference on Computer Vision*. 3615–3622. https://doi.org/10.1109/ICCV.2013.449

Timothy F. Cootes, Gareth J. Edwards, and Christopher J. Taylor. 2001. Active appearance models. *IEEE Transactions on pattern analysis and machine intelligence* 23, 6 (2001), 681–685.

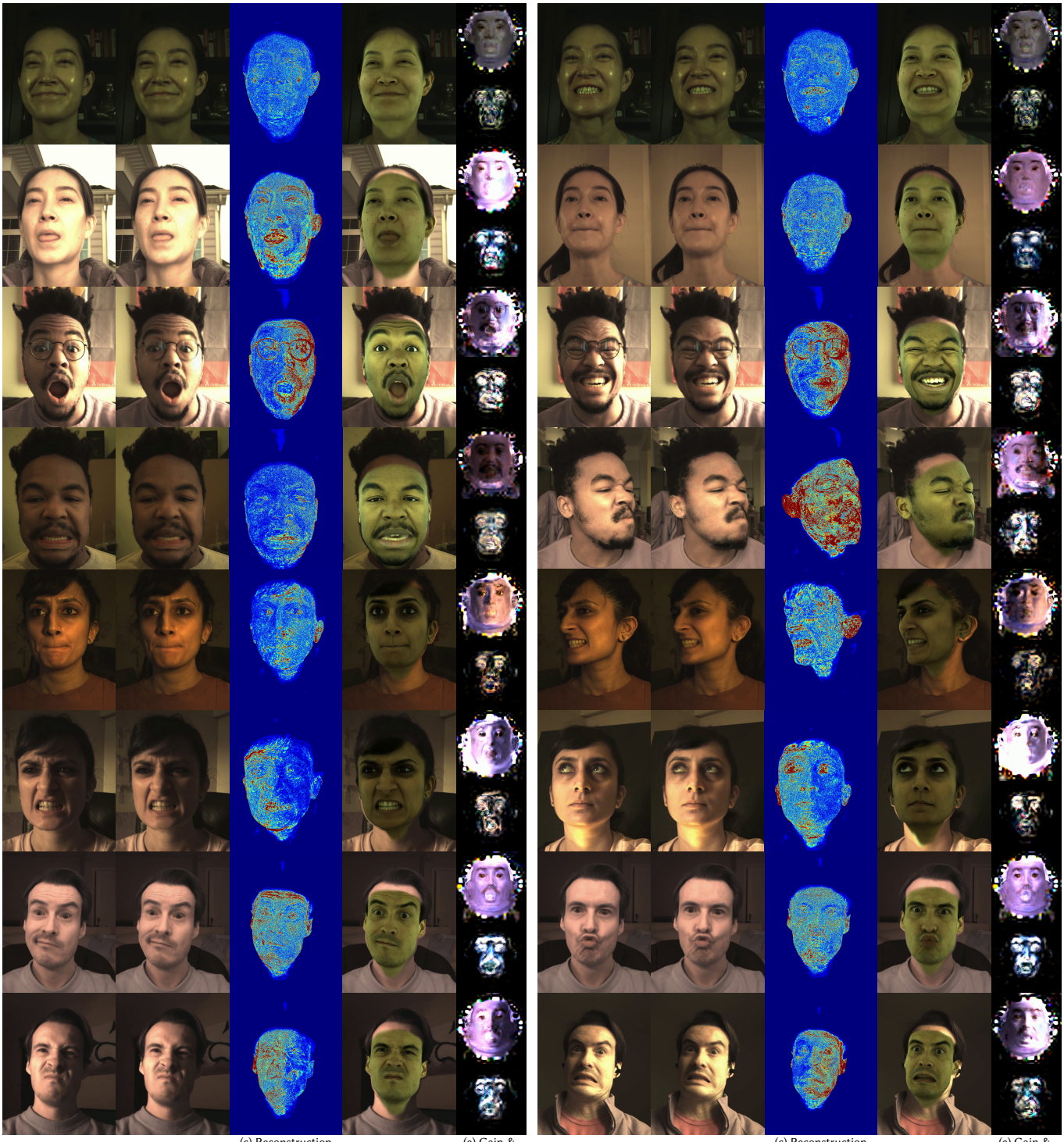

Fig. 17. Examples of off-line face model fitting on different users under different lighting conditions. With input image (a), our algorithm can decouple the accurate rigid head pose and non-rigid facial expression, and reconstruct the avatar with the same facial motions (d). The proposed lighting model can produce the gain and bias map (e), which reflects the lighting condition, head pose and facial expressions. These gain and bias map help to relight the avatar (b) which is pixel-wise matching the input image. We visualize the L_2 error between (a) and (b) as the reconstruction error in (c). Our method can handle different head poses or different lighting conditions, and well reconstruct both exaggerated and subtle facial expressions.

Fig. 18. Examples of real-time facial animations for different persons. With input image (a) our method can track 3D face and drive the avatar animation (b). Thanks to the view-dependent DAM representation, we can visualize the 3D avatar from different views (c). Our real-time facial animation method can handle different lighting conditions, recover expression to a wide range of motions. Our methods can well handle user with glasses on (bottom row).

Douglas Decarlo and Dimitris Metaxas. 2000. Optical flow constraints on deformable models with applications to face tracking. *International Journal of Computer Vision* 38, 2 (2000), 99–127.

Mingsong Dou, Philip Davidson, Sean Ryan Fanello, Sameh Khamis, Adarsh Kowdle, Christoph Rhemann, Vladimir Tankovich, and Shahram Izadi. 2017. Motion2Fusion: Real-time Volumetric Performance Capture. *SIGGRAPH Asia* (2017).

Mingsong Dou, Sameh Khamis, Yury Degtyarev, Philip Davidson, Sean Ryan Fanello, Adarsh Kowdle, Sergio Orts Escolano, Christoph Rhemann, David Kim, Jonathan Taylor, Pushmeet Kohli, Vladimir Tankovich, and Shahram Izadi. 2016. Fusion4D: Real-time Performance Capture of Challenging Scenes. *SIGGRAPH* (2016).

Graham Fyffe, Andrew Jones, Oleg Alexander, Ryosuke Ichikari, and Paul Debevec. 2014. Driving High-Resolution Facial Scans with Video Performance Capture. *ACM Transactions on Graphics (TOG)* 34, 1, Article 8 (Dec. 2014), 8:1–8:14 pages.

Thomas Gerig, Andreas Morel-Forster, Clemens Blumer, Bernhard Egger, Marcel Luthi, Sandro Schönborn, and Thomas Vetter. 2018. Morphable face models-an open framework. In *2018 13th IEEE International Conference on Automatic Face & Gesture Recognition (FG 2018)*. IEEE, 75–82.

Patrik Huber, Guosheng Hu, Rafael Tena, Pouria Mortazavian, P Koppen, William J Christmas, Matthias Ratsch, and Josef Kittler. 2016. A multiresolution 3d morphable face model and fitting framework. In *Proceedings of the 11th International Joint Conference on Computer Vision, Imaging and Computer Graphics Theory and Applications*.

Jing Xiao, S. Baker, I. Matthews, and T. Kanade. 2004. Real-time combined 2D+3D active appearance models. In *Proceedings of the 2004 IEEE Computer Society Conference on Computer Vision and Pattern Recognition, 2004. CVPR 2004.*, Vol. 2. II–II. https://doi.org/10.1109/CVPR.2004.1315210

F. Kahraman, M. Gokmen, S. Darkner, and R. Larsen. 2007. An Active Illumination and Appearance (AIA) Model for Face Alignment. In *2007 IEEE Conference on Computer Vision and Pattern Recognition*. 1–7. https://doi.org/10.1109/CVPR.2007.383399

Vahid Kazemi and Josephine Sullivan. 2014. One Millisecond Face Alignment with an Ensemble of Regression Trees. In *IEEE International Conference on Computer Vision and Pattern Recognition*.

Hyeongwoo Kim, Mohamed Elgharib, Hans-Peter Zollöfer, Michael Seidel, Thabo Beeler, Christian Richardt, and Christian Theobalt. 2019. Neural Style-Preserving Visual Dubbing. *ACM Transactions on Graphics (TOG)* 38, 6 (2019), 178:1–13.

Hyeongwoo Kim, Pablo Garrido, Ayush Tewari, Weipeng Xu, Justus Thies, Matthias Nießner, Patrick Pérez, Christian Richardt, Michael Zollöfer, and Christian Theobalt. 2018. Deep Video Portraits. *ACM Transactions on Graphics (TOG)* 37, 4 (2018), 163.

Hyeongwoo Kim, Michael Zollhöfer, Ayush Tewari, Justus Thies, Christian Richardt, and Christian Theobalt. 2017. InverseFaceNet: Deep Single-Shot Inverse Face Rendering From A Single Image. *CoRR* abs/1703.10956 (2017). arXiv:1703.10956 http://arxiv.org/abs/1703.10956

Diederik P Kingma and Max Welling. 2013. Auto-encoding variational bayes. *arXiv preprint arXiv:1312.6114* (2013).

Oliver Klehm, Fabrice Rousselle, Marios Papas, Derek Bradley, Christophe Hery, Bernd Bickel, Wojciech Jarosz, and Thabo Beeler. 2015. Recent Advances in Facial Appearance Capture. *Computer Graphics Forum (Proceedings of Eurographics - State of the Art Reports)* 34, 2 (May 2015), 709–733. https://doi.org/10/f7mb4b

Samuli Laine, Tero Karras, Timo Aila, Antti Herva, Shunsuke Saito, Ronald Yu, Hao Li, and Jaakko Lehtinen. 2017. Production-level Facial Performance Capture Using Deep Convolutional Neural Networks. In *Proceedings of the ACM SIGGRAPH / Eurographics Symposium on Computer Animation*. Article 10, 10 pages.

J. P. Lewis, Ken Anjyo, Taehyun Rhee, Mengjie Zhang, Fred Pighin, and Zhigang Deng. 2014. Practice and Theory of Blendshape Facial Models. In *Eurographics 2014 - State of the Art Reports*, Sylvain Lefebvre and Michela Spagnuolo (Eds.). The Eurographics Association. https://doi.org/10.2312/egst.20141042

Hao Li, Jihun Yu, Yuting Ye, and Chris Bregler. 2013. Realtime Facial Animation with On-the-Fly Correctives. *ACM Trans. Graph.* 32, 4, Article 42 (July 2013), 10 pages. https://doi.org/10.1145/2461912.2462019

Tianye Li, Timo Bolkart, Michael J Black, Hao Li, and Javier Romero. 2017. Learning a model of facial shape and expression from 4D scans. *ACM Trans. Graph.* 36, 6 (2017), 194–1.

Zhengqin Li, Zexiang Xu, Ravi Ramamoorthi, Kalyan Sunkavalli, and Manmohan Chandraker. 2018. Learning to reconstruct shape and spatially-varying reflectance from a single image. In *SIGGRAPH Asia 2018 Technical Papers*. ACM, 269.

Stephen Lombardi, Jason Saragih, Tomas Simon, and Yaser Sheikh. 2018. Deep Appearance Models for Face Rendering. *ACM Trans. Graph.* 37, 4, Article 68 (July 2018), 13 pages.

Ricardo Martin-Brualla, Rohit Pandey, Shuoran Yang, Pavel Pidlypenskyi, Jonathan Taylor, Julien Valentin, Sameh Khamis, Philip Davidson, Anastasia Tkach, Peter Lincoln, et al. 2018. Lookingood: Enhancing performance capture with real-time neural re-rendering. *arXiv preprint arXiv:1811.05029* (2018).

Iain Matthews and Simon Baker. 2004. Active appearance models revisited. *International journal of computer vision* 60, 2 (2004), 135–164.

S. McDonagh, M. Klaudiny, D. Bradley, T. Beeler, I. Matthews, and K. Mitchell. 2016. Synthetic Prior Design for Real-Time Face Tracking. In *International Conference on 3D Vision (3DV)*. 639–648.

Koki Nagano, Jaewoo Seo, Jun Xing, Lingyu Wei, Zimo Li, Shunsuke Saito, Aviral Agarwal, Jens Fursund, and Hao Li. 2018. PaGAN: Real-Time Avatars Using Dynamic Textures. *ACM Trans. Graph.* 37, 6, Article 258 (Dec. 2018), 12 pages. https://doi.org/10.1145/3272127.3275075

Kyle Olszewski, Joseph J. Lim, Shunsuke Saito, and Hao Li. 2016. High-fidelity Facial and Speech Animation for VR HMDs. *ACM Transactions on Graphics (TOG)* 35, 6, Article 221 (Nov. 2016), 14 pages.

Sergio Orts-Escolano, Christoph Rhemann, Sean Fanello, Wayne Chang, Adarsh Kowdle, Yury Degtyarev, David Kim, Philip L. Davidson, Sameh Khamis, Mingsong Dou, Vladimir Tankovich, Charles Loop, Qin Cai, Philip A. Chou, Sarah Mennicken, Julien Valentin, Vivek Pradeep, Shenlong Wang, Sing Bing Kang, Pushmeet Kohli, Yuliya Lutchyn, Cem Keskin, and Shahram Izadi. 2016. Holoportation: Virtual 3D Teleportation in Real-time. In *UIST*.

Rohit Pandey, Anastasia Tkach, Shuoran Yang, Pavel Pidlypenskyi, Jonathan Taylor, Ricardo Martin-Brualla, Andrea Tagliasacchi, George Papandreou, Philip Davidson, Cem Keskin, et al. 2019. Volumetric capture of humans with a single rgbd camera via semi-parametric learning. In *Proceedings of the IEEE Conference on Computer Vision and Pattern Recognition*. 9709–9718.

J. M. Saragih, S. Lucey, and J. F. Cohn. 2011. Real-time avatar animation from a single image. In *2011 IEEE International Conference on Automatic Face Gesture Recognition (FG)*. 213–220. https://doi.org/10.1109/FG.2011.5771400

Gabriel Schwartz, Shih-En Wei, Te-Li Wang, Stephen Lombardi, Tomas Simon, Jason Saragih, and Yaser Sheikh. 2020. The Eyes Have It: An Integrated Eye and Face Model for Photorealistic Facial Animation. *ACM Trans. Graph.* 39, 4, Article 91 (July 2020), 15 pages.

Soumyadip Sengupta, Angjoo Kanazawa, Carlos D Castillo, and David W Jacobs. 2018. SfSNet: Learning Shape, Reflectance and Illuminance of Facesin the Wild'. In *Proceedings of the IEEE Conference on Computer Vision and Pattern Recognition*. 6296–6305.

Karen Simonyan and Andrew Zisserman. 2014. Very deep convolutional networks for large-scale image recognition. *arXiv preprint arXiv:1409.1556* (2014).

J. Rafael Tena, Fernando De la Torre, and Iain Matthews. 2011. *Interactive Region-Based Linear 3D Face Models*. Association for Computing Machinery, New York, NY, USA. https://doi.org/10.1145/1964921.1964971

Ayush Tewari, Michael Zollöfer, Hyeongwoo Kim, Pablo Garrido, Florian Bernard, Patrick Perez, and Christian Theobalt. 2017. MoFA: Model-based Deep Convolutional Face Autoencoder for Unsupervised Monocular Reconstruction. In *IEEE International Conference on Computer Vision (ICCV)*.

J. Thies, M. Zollhöfer, M. Nießner, L. Valgaerts, M. Stamminger, and C. Theobalt. 2015. Real-time Expression Transfer for Facial Reenactment. *ACM Transactions on Graphics (TOG)* 34, 6 (2015).

Justus Thies, Michael Zollhöfer, Marc Stamminger, Christian Theobalt, and Matthias Nießner. 2016. Face2Face: Real-time Face Capture and Reenactment of RGB Videos. In *IEEE Conference on Computer Vision and Pattern Recognition (CVPR)*.

Justus Thies, Michael Zollhöfer, Christian Theobalt, Marc Stamminger, and Matthias Niessner. 2018. HeadOn: Real-Time Reenactment of Human Portrait Videos. *ACM Trans. Graph.* 37, 4, Article 164 (July 2018), 13 pages. https://doi.org/10.1145/3197517.3201350

Anh Tuan Tran, Tal Hassner, Iacopo Masi, and Gerard Medioni. 2017. Regressing Robust and Discriminative 3D Morphable Models with a very Deep Neural Network. In *Computer Vision and Pattern Recognition (CVPR)*.

Luan Tran, Feng Liu, and Xiaoming Liu. 2019. Towards High-fidelity Nonlinear 3D Face Morphable Model. In *In Proceeding of IEEE Computer Vision and Pattern Recognition*. Long Beach, CA.

Luan Tran and Xiaoming Liu. 2018. Nonlinear 3D Face Morphable Model. In *In Proceeding of IEEE Computer Vision and Pattern Recognition*. Salt Lake City, UT.

Georgios Tzimiropoulos, Joan Alabort-i Medina, Stefanos Zafeiriou, and Maja Pantic. 2013. *Generic Active Appearance Models Revisited*. Springer Berlin Heidelberg, Berlin, Heidelberg, 650–663.

Levi Valgaerts, Chenglei Wu, Andrés Bruhn, Hans-Peter Seidel, and Christian Theobalt. 2012. Lightweight Binocular Facial Performance Capture under Uncontrolled Lighting. In *ACM Transactions on Graphics (Proceedings of SIGGRAPH Asia 2012)*, Vol. 31. 187:1–187:11. https://doi.org/10.1145/2366145.2366206

Daniel Vlasic, Matthew Brand, Hanspeter Pfister, and Jovan Popović. 2005. Face Transfer with Multilinear Models. *ACM Trans. Graph.* 24, 3 (July 2005), 426–433. https://doi.org/10.1145/1073204.1073209

Shih-En Wei, Jason Saragih, Tomas Simon, Adam W. Harley, Stephen Lombardi, Michal Perdoch, Alexander Hypes, Dawei Wang, Hernan Badino, and Yaser Sheikh. 2019. VR Facial Animation via Multiview Image Translation. *ACM Trans. Graph.* 38, 4, Article 67 (July 2019), 16 pages. https://doi.org/10.1145/3306346.3323030

Thibaut Weise, Sofien Bouaziz, Hao Li, and Mark Pauly. 2011. *Realtime Performance-Based Facial Animation*. Association for Computing Machinery, New York, NY, USA. https://doi.org/10.1145/1964921.1964972

Xuehan Xiong and Fernando De la Torre. 2013. Supervised Descent Method and Its Applications to Face Alignment. In *Proceedings of the IEEE Conference on Computer Vision and Pattern Recognition (CVPR)*.

Jae Shin Yoon, Takaaki Shiratori, Shoou-I Yu, and Hyun Soo Park. 2019. Self-supervised adaptation of high-fidelity face models for monocular performance tracking. In *Proceedings of the IEEE Conference on Computer Vision and Pattern Recognition*. 4601–4609.

Alan Yuille and Daniel Kersten. 2006. Vision as Bayesian inference: analysis by synthesis? *Trends in cognitive sciences* 10, 7 (2006), 301–308.

Egor Zakharov, Aliaksandra Shysheya, Egor Burkov, and Victor Lempitsky. 2019. Few-shot adversarial learning of realistic neural talking head models. In *Proceedings of the IEEE International Conference on Computer Vision*. 9459–9468.

Richard Zhang. 2019. Making convolutional networks shift-invariant again. *arXiv preprint arXiv:1904.11486* (2019).

Michael Zollhöfer, Justus Thies, Pablo Garrido, Derek Bradley, Thabo Beeler, Patrick Pérez, Marc Stamminger, Matthias Nießner, and Christian Theobalt. 2018. State of the Art on Monocular 3D Face Reconstruction, Tracking, and Applications. *Computer Graphics Forum* (2018). https://doi.org/10.1111/cgf.13382